A Comparison of Optical and Near-Infrared Colours of Magellanic Cloud Star Clusters with Predictions of Simple Stellar Population Models

P. M. Pessev[1]*, P. Goudfrooij[1]*, T. H. Puzia[2]* and R. Chandar[3,4]*

[1] *Space Telescope Science Institute, 3700 San Martin Drive, Baltimore, MD 21218, U.S.A.*

[2] *Herzberg Institute of Astrophysics, 5071 West Saanich Road, Victoria, BC V9E 2E7, Canada*

[3] *The Observatories of the Carnegie Institution of Washington, 813 Santa Barbara Street, Pasadena, CA 91101-1292, U.S.A.*

[4] *Department of Physics and Astronomy, The University of Toledo, 2801 West Bancroft Street, Toledo, OH 43606, U.S.A.*

ABSTRACT

We present integrated JHK_s 2MASS photometry and a compilation of integrated-light optical photoelectric measurements for 84 star clusters in the Magellanic Clouds. These clusters range in age from ≈ 200 Myr to > 10 Gyr, and have [Fe/H] values from -2.2 to -0.1 dex. We find a spread in the intrinsic colours of clusters with similar ages and metallicities, at least some of which is due to stochastic fluctuations in the number of bright stars residing in low-mass clusters. We use 54 clusters with the most reliable age and metallicity estimates as test particles to evaluate the performance of four widely used SSP models in the optical/NIR colour-colour space. All models reproduce the reddening-corrected colours of the old ($\geqslant 10$ Gyr) globular clusters quite well, but model performance varies at younger ages. In order to account for the effects of stochastic fluctuations in individual clusters, we provide composite $B-V$, $B-J$, $V-J$, $V-K_s$ and $J-K_s$ colours for Magellanic Cloud clusters in several different age intervals. The accumulated mass for most composite clusters are higher than that needed to keep luminosity variations due to stochastic fluctuations below the 10% level. The colours of the composite clusters are clearly distinct in optical-NIR colour-colour space for the following intervals of age: > 10 Gyr, $2-9$ Gyr, $1-2$ Gyr, and 200 Myr-1 Gyr. This suggests that a combination of optical plus NIR colours can be used to differentiate clusters of different age and metallicity.

Key words: Magellanic Clouds, galaxies: star clusters, infrared: general, techniques: photometric

1 INTRODUCTION

The most efficient method to determine the age and metallicity for unresolved stellar systems (especially at high redshift) is by comparing their observed colours with the predictions of evolution synthesis models (e.g. Bruzual & Charlot 1993, 2003; Worthey 1994; Vazdekis 1999; Maraston 1998, 2005; Anders & Fritze-v. Alvensleben 2003). Thus, it is important to test the integrated colours predicted by recent models, based on objects which have accurate ages and metallicities determined independently. In the present paper we focus our attention on the combination of visual and near-infrared (NIR) photometry, which has proven to be

important for breaking the age-metallicity degeneracy, particularly in stellar populations older than $\approx$ a few times $\times$ 100 Myr (e.g. Goudfrooij et al. 2001; Puzia et al. 2002; Hempel & Kissler-Patig 2004).

With the advent of the *Spitzer Space Telescope (Spitzer)* and mid-infrared (MIR) instrumentation for some large ground-based telescopes, the NIR spectral region is now accessible at intermediate-to-high redshifts. In a recent paper based on *Spitzer* Infrared Array Camera (IRAC) imaging, van der Wel et al. (2006) reported significant discrepancies between some model predictions and the observed rest-frame K-band properties of early-type galaxies at z $\approx$ 1. Their results show that the interpretation of NIR photometry is hampered by model uncertainties. As a consequence the determination of masses of distant stellar systems based on

---

such data can have uncertainties up to a factor 2.5 (see Bruzual A. 2007).

Unfortunately, providing accurate model predictions in the near-infrared is challenging, since there are limitations imposed by the current lack of understanding of certain stages of stellar evolution (e.g., thermally pulsing asymptotic giant branch, or TP-AGB stars). These objects significantly affect the spectral energy distribution (SED) in the NIR and MIR for stellar populations with ages between ≈ 200 Myr to 3 Gyr. Another possible complication is that the stellar libraries used by population synthesis models contain mostly stars from the solar neighborhood. These stars have a star formation history which is not necessarily typical for extragalactic populations (e.g. relatively little variation of $[\alpha/Fe]$ ratios), and there are only a very limited number of AGB spectra available.

The Large and Small Magellanic Clouds (LMC and SMC respectively) provide a unique opportunity to test the accuracy of most current SSP models, since they contain a significant population of intermediate-age massive star clusters which are not easily accessible in our Galaxy. The ages and metallicities of these star clusters can be determined from deep colour-magnitude diagrams (CMDs) reaching below the main sequence turn-off (MSTO)[1]. Medium and high-resolution spectroscopy of individual giants in these clusters also provides independent metallicity estimates. Therefore their integrated-light properties (easily observed with small and moderate-aperture telescopes) can be combined with the accurate age/metallicity measurements and used to test (and calibrate) the SSP models.

In Pessev et al. (2006) (hereafter Paper I) we used the Two Micron All Sky Survey (2MASS; Skrutskie et al. (2006)) to derive NIR (JHK_s) integrated-light magnitudes and colours for a large sample of Magellanic Cloud star clusters, based on a homogeneous, accurately calibrated dataset. In the present study we use the sample from Paper I and new photometry for 9 additional objects (forming the largest dataset of integrated NIR magnitudes and colours of LMC/SMC star clusters to date) to test the performance of several SSP models. We combine the 2MASS data with optical photometry originating from the work of Bica et al. (1996) and the compilation of van den Bergh (1981). The technique adopted in Paper I - measuring JHK_s curves of growth to large radii allows us to utilize rather heterogeneous databases of optical photometry, usually performed with a set of fixed apertures. We use 54 clusters from our sample as "test particles". These clusters were chosen to have reliable age and metallicity measurements, covering a wide parameter space.

This paper is organized as follows: in §2 we define our extended sample and present the new photometry along with the compilation of visual magnitudes and colours. Four sets of SSP models are tested in §3, followed by concluding remarks in §4. Information about the properties of the cluster

Figure 1. A finding chart of the LMC showing the clusters in our sample. The R-band image is centred on $\alpha_{2000} = 05^h26^m37.7^s$ and $\delta_{2000} = -68°56'57.5"$. The arrow near the centre outlines the position of NGC 1928 ($\alpha_{2000} = 05^h20^m57.7^s$ and $\delta_{2000} = -69°28'40.2"$). This cluster is located close to the geometrical centre of the LMC bar, and was adopted by Bica et al. (1996) as a reference point for the relative coordinates of the LMC cluster system. The labeled arrows show the direction towards the clusters lying outside the boundaries of this chart. The R-band image (G. Bothun 1997, private communication) covers 8°x8°, while the dimensions of the chart are 16°x16°.
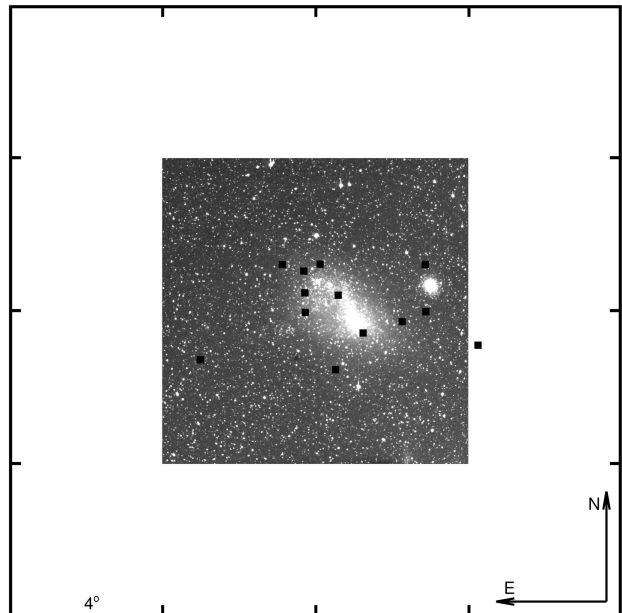
Figure 2. A finding chart of the SMC showing the clusters in our sample. The R-band image (G. Bothun 1997, private communication) is centred on $\alpha_{2000} = 01^h04^m42.8^s$ and $\delta_{2000} = -72°52'32.4"$. SMC clusters cover a smaller area than LMC objects. There is only one cluster outside the R frame, but for illustrational purposes the dimensions of this finder chart are identical to those of the LMC chart in Figure 1.

---

[1] Obtaining photometry with sufficient quality to secure reliable age and metallicity estimates for clusters in galaxies beyond the Magellanic Clouds requires a significant investment of observing time. To date only one such cluster, SKHB 312 in M31, has a CMD deep enough to probe the MSTO region (Brown et al. 2004). The photometry for this object was obtained as a result of a program utilizing 126 *Hubble Space Telescope (HST)* orbits.
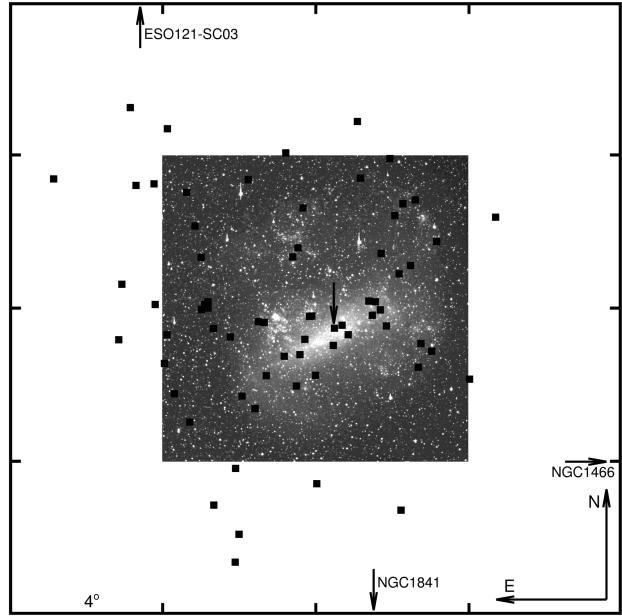
sample is presented in Appendices A and B. Transformations between the model grids in the Bessell & Brett (1988) system and the photometric system of 2 MASS are provided in Appendix C.

2 PHOTOMETRY OF MAGELLANIC CLOUD CLUSTERS

2.1 Extending the Sample - New Near-Infrared Integrated Photometry of Magellanic Cloud Clusters

We selected nine objects (see Table 1 for details) to add to our original sample which was presented in Paper I. The total sample now includes all of the old clusters in the Magellanic Clouds (with the exception of the Reticulum cluster, which is excluded due to insufficient depth of the available 2MASS images) and all of the "NIR-enhanced" clusters from Persson et al. (1983). Some objects were included in this extended sample because they have new integrated-light optical magnitudes and colours available. Overall the sample provides optimal coverage of the age-metallicity parameter space of MC star clusters. We intend to add 2MASS JHK_s integrated photometry for additional clusters as new information based on deep CMDs becomes available in the future.

The 2MASS (Skrutskie et al. 2006) atlas images were recovered through the interactive image service available on the survey web-page[2] (see Table 2 for information about the utilized images). We analysed these data following the reduction scheme presented in Paper I. Extinction corrections were derived using the online tools provided by the Magellanic Clouds Photometric Survey (MCPS, Zaritsky et al. (1997); details about extinction estimates for SMC and LMC are provided in Zaritsky et al. (2002) and Zaritsky et al. (2004) respectively. (A_v values and their uncertainties are listed in the last two columns of Table 1.)

All of the MC clusters with JHK_s NIR 2MASS photometry from Paper I and the present work are shown in the finder charts (see Figures 1 and 2 for the LMC and SMC, respectively). The cluster positions are marked by the centres of our aperture sets, derived as described in Paper I. Table 3 contains JHK_s photometry for the 9 new clusters[3].

Notes on individual objects – All the objects that required special attention during the reduction process are commented on below.

NGC 265 – This object is situated in a rich SMC star field and the depth of the images decreases from J to K_s. Analysis of the curves of growth show that for aperture diameters larger than $140''$ this trend causes some variation in the measured cluster colours. The photometry is carried out with the full set of apertures, but results for sizes exceeding $140''$ should be treated with caution.

NGC 1644 – This faint compact cluster is situated close to the edge of the atlas image. The photometry is carried out up to $90''$ aperture diameter. The curve of growth in K_s shows evidence for variations in the background level.

Results for aperture sizes larger than $60''$ could be affected by these variations. Due to the proximity of the image edge our automated procedure for deriving the aperture centres does not provide reliable results. Therefore the cluster centre was chosen "by eye", but we consider this position to be reliable due to the compactness of the object and lack of stellar contamination in the surrounding field.

NGC 1928 – This is an old globular cluster (see Mackey & Gilmore 2004). Situated in the LMC bar region, this object suffers from strong background/foreground contamination. Combined with the limited depth of the cluster's image on the 2MASS atlas frames, this makes the integrated photometry challenging. Due to the presence of several relatively bright stars in the vicinity of the cluster, we decided to use only the results based on the unresolved light from the object to derive the aperture centres. Several bright stars in the aperture set were subtracted after an analysis of their properties based on the infrared colours explained in detail in Paper I. The resulting integrated-photometry curves of growth show residual effects of the background removal and the NIR photometry should be treated with caution in this case.

NGC 2058 – This cluster is located close to the edge of the atlas image. Photometry is carried out with a set of apertures up to D=$80''$.

NGC 2107 – The cluster lies close to the edge of the atlas image. In this case photometry was carried out with a set of aperture sizes up to $140''$. The curves of growth indicate that we obtain good sampling of the flux from the object.

NGC 2108 – There are three luminous stars in the cluster. Their colours are consistent with those expected for carbon stars. It is noteworthy to mention that Ferraro et al. (2004) found the same number of AGB stars in their NIR photometric study of this object. The age estimates of the cluster are also consistent with the presence of carbon stars, so they are included in the final photometry.

NGC 2134 – Several luminous stars are present within the cluster area. They affect the centring, so we use the results from the unresolved component. The colours of these stars are consistent with those expected for carbon stars, and they are included in the final integrated photometry measurements.

NGC 2154 – Due to the proximity of the object to the edge of the atlas image, the photometry is carried out with a set of apertures up to $110''$ in diameter.

2.2 Compiling a Catalog of Optical Cluster Photometry

We conducted an extensive literature search for appropriate integrated optical cluster colours to combine with our NIR measurements. Our compilation from the literature is presented in Table 4. It is based on integrated-light photoelectric observations and lists the V magnitudes, $(B - V)$ and $(U - B)$ colours plus their uncertainties, reddening values towards the objects with their corresponding uncertainties are also included. The photometry comes from different observers, so special care was taken to ensure that the individual results are consistent. Recent independent CCD datasets from Goudfrooij et al. (2006) and Hunter et al. (2003) were also used in the consistency checks. The cases where discrep-

---

[2] http://irsa.ipac.caltech.edu/applications/2MASS/IM/interactive.html
[3] The listed magnitudes are not corrected for reddening.

Table 1. Extended Magellanic Cloud Cluster Sample

ID (1)	α_{2000} (2)	δ_{2000} (3)	Age, Errors & Ref				[Fe/H], Err & Ref			A_v (11)	ΔA_v (12)
			(4)	(5)	(6)	(7)	(8)	(9)	(10)		
NGC265	00:47:12	−73:28:38	8.5	+0.3	−0.3	2	−0.62	$^{+0.23}_{-0.61}$	2	0.34	0.02
NGC1644	04:37:39	−66:12:00	9.53	+0.05	−0.05	1	−1.4	±0.2	1	0.39	0.02
NGC1928	05:20:58	−69:28:40	10.11	+0.06	−0.08	5	−1.27	±0.14	5	0.34	0.06
NGC1994	05:28:22	−69:08:30	7.06			4				0.41	0.02
NGC2058	05:36:55	−70:09:44	7.85	+0.10	−0.15	4				0.39	0.02
NGC2107	05:43:13	−70:38:23	8.55	+0.25	−0.24	3				0.36	0.04
NGC2108	05:43:56	−69:10:48	8.90	+0.26	−0.26	3				0.50	0.05
NGC2134	05:51:56	−71:05:54	8.27			7	−0.4		7	0.62	0.03
NGC2154	05:57:38	−67:15:42	9.16	+0.28	−0.28	3	−0.56	±0.2	6	0.39	0.03

Notes to Table 1: Column (1): Object ID. Columns (2) and (3): Cluster coordinates - Right Ascension (given as hours, minutes, seconds) and Declination (degrees, minutes, seconds) in J2000 retrieved from Simbad Astronomical Database. Column (4): age of the object given as *log(age)* with corresponding errors in columns (5) and (6) and literature references (see bellow) in (7). Column (8): metallicity values retrieved from the literature with their errors (9) and references (10). Column (11): *V* band reddening values for the objects with corresponding errors (12) retrieved from the MCPS reddening estimation tool.
References: (1) Bica et al. (1986) (2) Chiosi & Vallenari (2007) (3) Elson & Fall (1985) (4) Elson & Fall (1988) (5) Mackey & Gilmore (2004) (6) Olszewski et al. (1991) (7) Vallenari et al. (1994)

Table 2. 2MASS Atlas Images of the Clusters in the Extended Sample.

ID (1)	N (2)	J (3)	H (4)	K_s (5)
NGC265	1	aJ_asky_980809s0810198.fits	aH_asky_980809s0810198.fits	aK_asky_980809s0810198.fits
NGC1644	1	aJ_asky_991026s1140257.fits	aH_asky_991026s1140257.fits	aK_asky_991026s1140257.fits
NGC1928	1	aJ_asky_981220s0850162.fits	aH_asky_981220s0850162.fits	aK_asky_981220s0850162.fits
NGC1994	1	aJ_asky_000212s0190150.fits	aH_asky_000212s0190150.fits	aK_asky_000212s0190150.fits
NGC2058	1	aJ_asky_000206s0240186.fits	aH_asky_000206s0240186.fits	aK_asky_000206s0240186.fits
NGC2107	1	aJ_asky_980321s0080209.fits	aH_asky_980321s0080209.fits	aK_asky_980321s0080209.fits
NGC2108	1	aJ_asky_980321s0080150.fits	aH_asky_980321s0080150.fits	aK_asky_980321s0080150.fits
NGC2134	1	aJ_asky_981025s1000044.fits	aH_asky_981025s1000044.fits	aK_asky_981025s1000044.fits
NGC2154	1	aJ_asky_981025s1110068.fits	aH_asky_981025s1110068.fits	aK_asky_981025s1110068.fits

Notes to Table 2: Column (1): Object ID. Column (2): Number of image sets retrieved. Columns (3), (4) and (5): designations of the individual J, H and K_s frames.

ancies cannot be readily explained are listed as notes in the last column of Table 4. As a rule, we provide information about the largest aperture size available. This reduces the effects of both the aperture centring (which could differ for the optical and NIR data), the stochastic fluctuations of the background stellar population and of the stars in the clusters themselves. The photometry of all SMC clusters is taken from the homogeneous dataset of Alcaino (1978), and is also listed in Table 4. Reddening information is compiled from a number of sources (indicated in the table) and preference is given to values based on deep CMDs.

3   TESTING THE MODELS

In recent years significant improvements in modeling the properties of Simple Stellar Populations have been achieved, and several independent sets of SSP models have been published. Here, we will focus our attention on comparing the models by Vazdekis, Bruzual & Charlot, Anders & Fritze-v. Alvensleben, and Maraston with the integrated photometry

of Magellanic Cloud clusters presented in paper I and in this work. Our main goals are to: *(i)* determine which models best reproduce the observed cluster colours; *(ii)* establish whether clusters of different ages and metallicities can be accurately distinguished via a combination of optical-NIR colours; and *(iii)* provide information that could help improve the model predictions. Below, we first briefly discuss the colours we will use to compare observed data with SSP model predictions as well as the NIR photometric system we will adopt in that context. We then present the actual comparisons between data and SSP model predictions for distinct age groups. The selection of clusters for each age group is described in Appendices A and B.

3.1   Choice of Optical-NIR colours

To select a set of optical-NIR colours that are most applicable for a proper and meaningful comparison between observed data and SSP model predictions, we look for colours that do a good job at breaking the well-known age-

Table 3. New NIR photometry of Magellanic Cloud clusters

ID (1)	α_{2000} (2)	δ_{2000} (3)	d (4)	Flag (5)	D (6)		J (7)	Jerr (8)	H (9)	Herr (10)	K_s (11)	$K_s err$ (12)
NGC265	00:47:09.9	-73:28:39.3	7.5	AAB	20		13.00	0.03	12.43	0.03	12.53	0.05
					40		11.80	0.03	10.48	0.02	10.41	0.02
					60		11.54	0.06	10.31	0.03	10.27	0.05
					80		11.35	0.08	10.15	0.05	10.04	0.06
					100		11.16	0.11	10.05	0.07	9.92	0.09
					120		10.96	0.13	9.90	0.09	9.79	0.12
					140		10.78	0.15	9.84	0.12	9.71	0.15
					160	:	10.42	0.14	9.61	0.12	9.64	0.18
					180	:	10.32	0.17	9.52	0.15	9.50	0.21
					200	:	10.18	0.19	9.44	0.17	9.42	0.24
NGC1644	04:37:39.8	-66:11:55.5	6.5	BBB	20		12.08	0.03	11.62	0.02	11.43	0.02
					40		11.51	0.06	11.05	0.05	10.84	0.05
					60		11.31	0.11	10.88	0.10	10.76	0.10
					80	:	11.12	0.17	10.74	0.16	10.61	0.16
					90	:	11.05	0.20	10.66	0.18	10.51	0.18
NGC1928	05:20:57.8	-69:28:41.2	1	AAB	20		11.65	0.03	11.05	0.03	11.24	0.04
					40		11.04	0.05	10.51	0.06	10.56	0.09
					60		10.73	0.08	10.28	0.11	10.25	0.15
					80		10.54	0.12	10.10	0.17	9.34	0.11
					100		10.40	0.17	9.98	0.24	9.24	0.16
					120		10.17	0.20	9.73	0.28	9.06	0.20
					140		10.05	0.25	9.60	0.35	8.75	0.21
					160		9.73	0.24	9.16	0.30	8.69	0.26
					180		9.49	0.25	8.78	0.27	8.54	0.29
					200		9.35	0.28	8.70	0.32	8.47	0.34
NGC1994	05:28:22.4	-69:08:31.3	2	BBA	20		8.33	0.01	7.63	0.01	7.45	0.01
					40		8.28	0.01	7.59	0.01	7.40	0.01
					60		8.25	0.01	7.57	0.01	7.38	0.01
					80		8.22	0.02	7.55	0.01	7.36	0.01
					100		8.14	0.02	7.47	0.01	7.35	0.02
					120		7.95	0.03	7.26	0.02	7.14	0.02
					140		7.80	0.03	7.10	0.02	6.95	0.03
					160		7.78	0.04	7.09	0.02	6.93	0.04
					180		7.76	0.05	7.07	0.03	6.92	0.04
					200		7.74	0.05	7.06	0.04	6.91	0.05
NGC2058	05:36:54.0	-70:09:42.0	10	BBB	20		10.72	0.02	10.15	0.01	10.08	0.02
					40		9.82	0.03	9.22	0.02	9.17	0.03
					60		9.57	0.04	9.03	0.04	8.95	0.05
					80		9.26	0.06	8.76	0.06	8.60	0.07
NGC2107	05:43:13.3	-70:38:29.8	2.5	BBB	20		10.81	0.03	9.98	0.02	9.70	0.02
					40		10.21	0.07	9.54	0.04	9.31	0.05
					60		10.05	0.13	9.43	0.08	9.20	0.11
					80		9.90	0.20	9.35	0.14	9.12	0.18
					100		9.70	0.26	9.14	0.18	8.92	0.24
					120		9.47	0.31	8.87	0.20	8.63	0.27
					140		9.34	0.39	8.72	0.24	8.32	0.27
NGC2108	05:43:56.7	-69:10:49.9	4	BBB	20		12.31	0.02	11.23	0.01	10.97	0.01
					40		10.78	0.01	9.88	0.01	9.36	0.01
					60		10.48	0.02	9.71	0.02	9.25	0.01
					80		10.35	0.03	9.63	0.03	9.20	0.02
					100		10.26	0.03	9.56	0.04	9.15	0.03
					120		10.17	0.04	9.47	0.05	9.10	0.05
					140		10.00	0.05	9.31	0.06	9.00	0.06
					160		9.55	0.05	8.83	0.05	8.45	0.04
					180		9.50	0.05	8.81	0.06	8.41	0.06
					200		9.45	0.06	8.77	0.08	8.39	0.07

Notes to Table 3. See next page

Table 3. Continued

ID (1)	α_{2000} (2)	δ_{2000} (3)	d (4)	Flag (5)	D (6)	J (7)	$Jerr$ (8)	H (9)	$Herr$ (10)	K_s (11)	$K_s err$ (12)
NGC2134	05:51:56.5	-71:05:50.4	4.5	BBB	20	10.80	0.01	10.16	0.01	10.10	0.01
					40	10.18	0.02	9.68	0.01	9.65	0.01
					60	9.94	0.03	9.50	0.02	9.43	0.02
					80	9.78	0.04	9.39	0.03	9.25	0.03
					100	9.46	0.04	8.96	0.03	8.77	0.03
					120	9.42	0.06	8.93	0.05	8.74	0.05
					140	8.95	0.05	8.31	0.04	8.01	0.03
					160	8.86	0.06	8.22	0.04	7.89	0.04
					180	8.82	0.08	8.16	0.05	7.85	0.05
					200	8.82	0.10	8.18	0.07	7.86	0.06
NGC2154	05:57:37.9	-67:15:43.7	2.0	BAB	20	11.24	0.01	10.38	0.01	9.86	0.01
					40	10.44	0.01	9.64	0.01	9.18	0.01
					60	10.16	0.02	9.38	0.01	8.92	0.01
					80	9.94	0.02	9.22	0.02	8.79	0.01
					100	9.80	0.03	9.11	0.02	8.68	0.02
					110	9.78	0.04	9.11	0.03	8.68	0.02

Notes to Table 3: Column (1) is the cluster designation, (2) and (3) are the right ascension and declination of the position used to centre the apertures for the integral photometry ((hh:mm:ss.s) and (dd:mm:ss.s) respectively). Column (4) is the offset (in arcseconds) measured on 2MASS images between that position and the cluster coordinates retrieved from SIMBAD. Column (5) contains a flag, providing information about the age (first letter), metalicity estimates (second letter) and the photometry (third letter) for each cluster. A is corresponding to a reliable age, metallicity and photometry, B denotes the cases when the age and metallicity values are uncertain and when used in the third position B stands for the cases described in Section 2.1 and/or the photometry was provided in aperture sizes smaller than 200″. The aperture diameters (arcseconds) used for each measurement are listed in column (6), they are denoted with colon in case complications with photometry were suspected. The photometry information (uncorrected for reddening) is given in columns (7) – (12), in the order: J magnitude, photometric uncertainty in J, and the same information for the other two survey bands H and K_s. The photometric uncertainty in each band is calculated as the quadrature sum of the zero point uncertainty, internal uncertainty of the photometry, and the uncertainty due to stochastic fluctuations of the background stellar population.

metallicity degeneracy while typically delivering photometry with adequate signal-to-noise (S/N) ratios. For this purpose we follow the work of Puzia et al. (2007) who showed that the colour combination $B - J$ vs. $J - K$ provides very good age resolution (through $B - J$) while $J - K$ is much more sensitive to metallicity than to age (except during a brief age interval after the AGB phase transition where $J - K$ shows a modest age dependence; see also Ferraro et al. 2000). In addition, we present $V - J$ vs. $J - K$ colour-colour diagrams since the V-band typically provides a higher S/N in observations than the B band.

3.2 Stochastic Effects in the Stellar Populations

When a comparison between observations of star clusters and theoretical predictions is performed, it is important to keep in mind that models assume that clusters are sufficiently massive that all stages of stellar evolution are well sampled. Predictions of any model based on these assumptions will match the observations only in the limit of a sufficiently large number of observed stars. The mass of real stellar systems thus drives the validity of comparison with model predictions.

The level of stochastic fluctuations which arise at different total cluster masses has been addressed in a number of previous studies (e.g. Bruzual A. 2002; Lançon & Mouhcine 2000; Cerviño & Luridiana 2004). Most notably, Lançon & Mouhcine calculate the minimum masses of a stellar popu-

lation with solar metallicity that ensure that the luminosity fluctuations are less than 10% of the mean luminosity ($\mathcal{M}_{(10\%)}$), $\sigma_L/L \leqslant 10\%$ (roughly corresponding to $\sigma = 0.1$ mag) for several photometric passbands. Cerviño & Luridiana (2004) define a "Lowest Luminosity Limit" (LLL) which requires that the total luminosity of a modeled cluster be larger than the contribution of the brightest star included in the isochrones, and show that the highest LLL masses are derived for the K band. Any object which complies with these mass limits provides a meaningful comparison for the entire range of optical-NIR colours in our study. Below, we check whether our composite clusters are more massive than the implied LLL masses by comparing the most luminous star in the isochrone (at the mean age and metallicity of each composite cluster) with the estimated cluster mass (described below). Using the on-line tool CMD 1.2l[4] provided by L. Girardi, we adopt a Kroupa (2001) IMF corrected for binaries (his Equation 6), and find that all of our composite cluster easily satisfy the less stringent LLL criterion. The LLL masses that we use are given in Table 6, and have been corrected for the difference in the adopted lower mass limits (0.01 $M_\odot$ in Cerviño & Luridiana and 0.1 $M_\odot$ in this work). Cerviño & Luridiana (2004) compare their values of LLL with the $\mathcal{M}_{(10\%)}$ masses derived by Lançon & Mouhcine, scaled for differences in the adopted IMF between the two works. These scaled values of $\mathcal{M}_{(10\%)}$ are also presented in

---

[4] available at: http://stev.oapd.inaf.it/ lgirardi/cgi-bin/cmd

Table 4. Compilation of Optical Photometry

ID (1)	Galaxy (2)	D (3)	V (4)	$(B-V)$ (5)	$(U-B)$ (6)	Ref. (7)	A_V (8)	Ref. (9)	SWB (10)	Note (11)
NGC121	SMC	62	11.24 ± 0.01	0.76 ± 0.00	0.10 ± 0.01	1	0.16 ± 0.09	11	VII	
NGC152	SMC	62	12.94 ± 0.04	0.70 ± 0.02	0.18 ± 0.02	1	0.16 ± 0.03	7	V	
NGC265	SMC	62	12.13 ± 0.03	0.30 ± 0.01	-0.11 ± 0.05	1	$0.19 ^{+\,0.15}_{-\,0.13}$	6	III	
NGC330	SMC	62	9.60 ± 0.01	0.15 ± 0.01	-0.46 ± 0.00	1	0.37 ± 0.02	-	I	
NGC339	SMC	62	12.84 ± 0.04	0.73 ± 0.01	0.03 ± 0.00	1	0.09 ± 0.12	11	VII	
NGC361	SMC	62	12.24 ± 0.01	0.78 ± 0.00	0.14 ± 0.02	1	0.22 ± 0.09	11	VII	
NGC411	SMC	62	12.21 ± 0.04	0.62 ± 0.01	0.24 ± 0.02	1	0.37 ± 0.03	7	V	
NGC416	SMC	62	11.42 ± 0.00	0.73 ± 0.00	0.12 ± 0.00	1	0.25 ± 0.09	10	VII	
NGC419	SMC	62	10.61 ± 0.01	0.65 ± 0.01	0.24 ± 0.01	1	0.20 ± 0.02	-	V	
NGC458	SMC	62	11.73 ± 0.03	0.16 ± 0.00	-0.17 ± 0.01	1	0.32 ± 0.02	-	V	
NGC1466	LMC	60	11.59 ± 0.03	0.68 ± 0.02	0.13 ± 0.03	15	0.28 ± 0.06	16	VII	
NGC1644	LMC	60	12.89 ± 0.02	0.60 ± 0.03	0.19 ± 0.02	15	0.39 ± 0.02	-	V	
NGC1651	LMC	100	12.28 ± 0.04	0.71 ± 0.04	0.28 ± 0.04	4	0.34 ± 0.03	8	V	
NGC1711$_{(B)}$	LMC	50	12.50 ± 0.04	0.27 ± 0.04	-0.04 ± 0.04	4	0.56 ± 0.01	-	III	1
NGC1711$_{(v)}$	LMC	60	10.11 ± 0.03	0.12 ± 0.01	-0.37 ± 0.02	15			III	1
NGC1718	LMC	62	12.25 ± 0.01	0.76 ± 0.01	0.26 ± 0.02	2	0.31 ± 0.09	8	VI	
NGC1751	LMC	100	11.73 ± 0.04	0.79 ± 0.04	0.27 ± 0.04	4	0.65 ± 0.06	-	VI	
NGC1754	LMC	100	11.57 ± 0.04	0.75 ± 0.04	0.15 ± 0.04	4	0.28 ± 0.06	12	VII	
NGC1777	LMC	38	12.80 ± 0.02	0.60 ± 0.03	0.17 ± 0.03	4	0.31 ± 0.09	8	IVB	
NGC1783	LMC	60	10.97 ± 0.02	0.63 ± 0.02	0.20 ± 0.03	15	0.30 ± 0.03	-	V	
NGC1786$_{(u)}$	LMC	60	10.16 ± 0.04	0.67 ± 0.00	0.06 ± 0.02	15	0.28 ± 0.16	5	VII	2
NGC1786$_{(c)}$	LMC	60	10.88 ± 0.04	0.74 ± 0.00	0.10 ± 0.02	15			VII	2
NGC1805	LMC	60	10.63 ± 0.03	0.11 ± 0.02	-0.55 ± 0.01	15	0.32 ± 0.02	-	I	
NGC1806	LMC	60	11.27 ± 0.04	0.26 ± 0.02	0.73 ± 0.02	15	0.25 ± 0.04	-	V	
NGC1818	LMC	60	9.85 ± 0.02	0.18 ± 0.02	-0.46 ± 0.00	15	0.39 ± 0.02	-	I	
NGC1831	LMC	60	11.18 ± 0.02	0.34 ± 0.02	0.13 ± 0.02	15	0.34 ± 0.03	8	IVA	
NGC1835	LMC	60	10.16 ± 0.05	0.74 ± 0.04	0.11 ± 0.03	15	0.25 ± 0.06	12	VII	
NGC1841	LMC	25	14.08	0.90	0.50	14	0.62 ± 0.09	5	VII	
NGC1846	LMC	60	11.40 ± 0.02	0.31 ± 0.05	0.74 ± 0.03	15	0.41 ± 0.04	-	VI	
NGC1847	LMC	72	11.06 ± 0.02	0.20 ± 0.02	-0.33 ± 0.03	3	0.49 ± 0.02	-	I	
NGC1850	LMC	60	9.36 ± 0.06	0.11 ± 0.03	-0.34 ± 0.07	15	0.33 ± 0.01	-	II	
NGC1856	LMC	60	10.07 ± 0.02	0.34 ± 0.01	0.06 ± 0.01	15	0.65 ± 0.06	8	IVA	
NGC1860	LMC	72	11.04 ± 0.02	0.14 ± 0.02	-0.39 ± 0.03	3	0.22 ± 0.03	-	I	
NGC1866	LMC	60	9.89 ± 0.01	0.26 ± 0.02	-0.06 ± 0.01	15	0.28 ± 0.06	-	III	
NGC1868	LMC	62	11.57 ± 0.02	0.45 ± 0.02	0.15 ± 0.03	3	0.12 ± 0.03	8	IVA	
NGC1898	LMC	60	11.52 ± 0.06	0.75 ± 0.02	-0.03 ± 0.03	15	0.22 ± 0.06	12	VII	
NGC1916	LMC	44	10.38 ± 0.02	0.78 ± 0.02	0.18 ± 0.03	3	0.42 ± 0.05	-	VII	
NGC1928	LMC	62	11.88 ± 0.02	0.22 ± 0.02	-0.31 ± 0.03	3	0.20 ± 0.05	9	VII	
NGC1939	LMC	38	11.78 ± 0.05	0.69 ± 0.05	0.09 ± 0.05	4	0.40 ± 0.08	9	VII	
NGC1978	LMC	60	10.74 ± 0.04	0.78 ± 0.04	0.23 ± 0.07	15	0.76 ± 0.05	-	VI	
NGC1984	LMC	50	9.99 ± 0.04	0.01 ± 0.04	-0.82 ± 0.04	4	0.36 ± 0.02	-	0	
NGC1987	LMC	60	12.18 ± 0.01	0.51 ± 0.01	0.18 ± 0.02	15	0.28 ± 0.03	-	IVB	
NGC1994	LMC	50	9.78 ± 0.04	0.09 ± 0.04	-0.69 ± 0.04	4	0.41 ± 0.02	-	I	
NGC2004	LMC	72	9.60 ± 0.02	0.13 ± 0.02	-0.71 ± 0.03	3	0.33 ± 0.02	-	I	
NGC2005	LMC	25	11.57 ± 0.00	0.73 ± 0.00	0.20 ± 0.00	14	0.37 ± 0.06	12	VII	
NGC2011	LMC	45	10.58 ± 0.02	0.00 ± 0.02	-0.72 ± 0.02	3	0.47 ± 0.02	-	I	
NGC2019	LMC	60	10.95 ± 0.01	0.77 ± 0.01	0.16 ± 0.02	15	0.37 ± 0.06	12	VII	
NGC2031	LMC	72	10.83 ± 0.02	0.26 ± 0.02	-0.07 ± 0.03	3	0.40 ± 0.03	-	III	
NGC2058$_{(v)}$	LMC	60	11.85 ± 0.04	0.24 ± 0.01	-0.12 ± 0.01	15	0.39 ± 0.02	-	III	3
NGC2058$_{(G)}$	LMC	60	10.73 ± 0.03						III	3
NGC2100	LMC	60	9.60 ± 0.04	0.16 ± 0.02	-0.56 ± 0.02	15	0.80 ± 0.02	-	I	
NGC2107	LMC	60	11.51 ± 0.02	0.38 ± 0.03	0.13 ± 0.03	15	0.36 ± 0.04	-	IVA	
NGC2108	LMC	62	12.32 ± 0.01	0.58 ± 0.01	0.22 ± 0.02	2	0.50 ± 0.05	-	IVB	
NGC2121	LMC	62	12.37 ± 0.01	0.84 ± 0.01	0.25 ± 0.02	2	0.22 ± 0.06	8	VI	
NGC2134	LMC	60	11.05 ± 0.04	0.26 ± 0.02	-0.02 ± 0.03	15	0.62 ± 0.03	-	III	
NGC2136	LMC	60	10.54 ± 0.02	0.28 ± 0.02	-0.13 ± 0.02	15	0.58 ± 0.02	-	III	
NGC2153	LMC	100	13.05 ± 0.04	0.69 ± 0.04	0.03 ± 0.04	4	0.27 ± 0.05	-	VII	
NGC2154	LMC	62	12.32 ± 0.01	0.68 ± 0.01	0.24 ± 0.02	2	0.39 ± 0.03	-	V	
NGC2155	LMC	62	12.60 ± 0.01	0.81 ± 0.01	0.23 ± 0.02	2	0.06 ± 0.03	8	VI	
NGC2156	LMC	72	11.38 ± 0.02	0.12 ± 0.02	-0.07 ± 0.03	3	0.20 ± 0.02	-	III	
NGC2157	LMC	60	10.16 ± 0.02	0.19 ± 0.02	-0.16 ± 0.01	15	0.42 ± 0.02	-	III	

Notes to Table 4. See next page

Table 4. Continued

ID (1)	Galaxy (2)	D (3)	V (4)	$(B-V)$ (5)	$(U-B)$ (6)	Ref. (7)	A_V (8)	Ref. (9)	SWB (10)	Note (11)
NGC2159	LMC	72	11.38 ± 0.02	0.28 ± 0.02	-0.14 ± 0.03	3	0.29 ± 0.03	-	III	
NGC2162	LMC	62	12.70 ± 0.01	0.68 ± 0.01	0.31 ± 0.02	2	0.09 ± 0.06	8	V	
NGC2164	LMC	60	10.34 ± 0.01	0.10 ± 0.01	-0.24 ± 0.01	6	0.33 ± 0.02	-	II	
NGC2172	LMC	72	11.75 ± 0.02	0.18 ± 0.02	-0.16 ± 0.03	3	0.26 ± 0.03	-	III	
NGC2173	LMC	150	11.88 ± 0.05	0.82 ± 0.05	0.28 ± 0.05	4	0.22 ± 0.06	8	VI	
NGC2190	LMC	61	12.94 ± 0.02	0.63 ± 0.03	0.29 ± 0.03	4	0.39 ± 0.02	-	V	
NGC2193	LMC	38	13.42 ± 0.02	0.71 ± 0.03	0.20 ± 0.03	4	0.39 ± 0.02	-	V	
NGC2203	LMC	150	11.29 ± 0.04	0.77 ± 0.04	0.26 ± 0.04	4	0.39 ± 0.02	-	VI	
NGC2209	LMC	62	13.15 ± 0.01	0.52 ± 0.01	0.36 ± 0.02	2	0.47 ± 0.09	8	IVB	
NGC2210	LMC	60	10.94 ± 0.03	0.71 ± 0.03	0.11 ± 0.01	6	0.28 ± 0.09	5	VII	
NGC2213	LMC	62	12.38 ± 0.01	0.71 ± 0.01	0.28 ± 0.02	2	0.19 ± 0.09	8	V	
NGC2214	LMC	60	10.93 ± 0.01	0.11 ± 0.02	-0.27 ± 0.01	6	0.39 ± 0.02	-	II	
NGC2231	LMC	44	13.20 ± 0.01	0.67 ± 0.01	0.24 ± 0.02	2	0.39 ± 0.02	-	V	
NGC2249	LMC	72	12.23 ± 0.02	0.43 ± 0.02	0.20 ± 0.03	3	0.03 ± 0.06	8	IVB	
NGC2257	LMC	61	12.62 ± 0.02	0.62 ± 0.03	0.01 ± 0.03	4	0.00 ± 0.00	13	VII	
ESO121-003	LMC	61	14.04 ± 0.02	0.87 ± 0.03	0.17 ± 0.05	4	0.10 ± 0.05	9	VII	
Hodge4	LMC	38	13.33 ± 0.02	0.66 ± 0.03	0.16 ± 0.05	4	0.39 ± 0.02	-	V	
Hodge11	LMC	62	11.98 ± 0.01	0.63 ± 0.01	0.00 ± 0.02	2	0.23 ± 0.02	10	VII	
Hodge14	LMC	62	13.42 ± 0.01	0.72 ± 0.01	0.21 ± 0.02	2	0.25 ± 0.06	8	V	
Kron3	SMC	62	12.05 ± 0.02	0.69 ± 0.01	0.05 ± 0.02	1	0.00 ± 0.06	11	VII	
Lindsay1	SMC	62	13.32 ± 0.05	0.75 ± 0.00	0.17 ± 0.05	1	0.19 ± 0.06	11	VII	
Lindsay113	SMC	62	13.61 ± 0.04	0.73 ± 0.02	0.05 ± 0.09	1	0.00 ± 0.06	11	VII	
LW431	LMC	38	13.67 ± 0.02	0.74 ± 0.03	0.13 ± 0.05	4	0.39 ± 0.02	-	VII	
SL842	LMC	38	14.15 ± 0.02	0.79 ± 0.03	0.11 ± 0.05	4	0.39 ± 0.02	-	VII	

Notes on Table 4: Column (1) is the cluster designation, (2) gives the galaxy in which the object resides. The diameter of the aperture used for the integral visual magnitude and colour measurements is given in column (3). Column (4) gives the V magnitude and it's uncertainty, while (5) and (6) list $(B-V)$ and $(U-B)$ colours and their corresponding uncertainties. These values are not reddening corrected. References to the sources of the integrated-light measurements are listed in column (7). Column (8) presents A_V information and corresponding uncertainties. References to the reddening information are given in column (9). Preference is given to extinction estimates based on deep CMDs. In case these were not available, extinction values retrieved from the website of Magellanic Clouds Photometric Survey are provided (marked with dashes in column (9)). Column (10) shows the SWB type of the object, for the LMC clusters the information comes from Bica et al. (1996), SWB types of SMC clusters were recovered from from the *s*-parameter calibration of Elson & Fall (1985). Finally some remarks to the objects or the photometry are given in column (11).

NOTES ON COLUMN (11): (1) The information about this object in Bica et al. (1996) and van den Bergh & Hagen (1968) is completely discrepant with each other. Both values are listed with lowercase "B" and "v" added in parenthesis to the cluster designation.

(2) There is a foreground star superposed on the object. The flux from the star and part of the cluster were measured in a $15''$ diaphragm and were subtracted from the flux of the larger (D=$60''$) aperture encompassing the object to derive the final colours and magnitudes. The uncorrected and corrected values are listed in lowercase "u" and "c" in parenthesis after the cluster designation, respectively. All the data is from van den Bergh & Hagen (1968). The photometric uncertainties for the uncorrected mesurements are also adopted for the corrected ones. They should be considered a lower limit.

(3) Measurements for NGC 2058 from Goudfrooij et al. (2006) and van den Bergh & Hagen (1968) are discrepant by more than one magnitude in V. A possible explanation is misidentification of the object in the earlier study. Inspection of a $14' \times 14'$ V image available in SIMBAD revealed several less luminous clusters in close proximity to the object, which might have caused the overestimate of the V magnitude in van den Bergh & Hagen. The V value from Goudfrooij et al. is also listed in the table. Lowercase "G" and "v" are added in parenthesis to the cluster designation to indicate the origin of the photometry (Goudfrooij et al. (2006) and van den Bergh & Hagen (1968) respectively).

References: (1)Alcaino (1978) (2)Bernard (1975) (3)Bernard & Bigay (1974) (4)Bica et al. (1996) (5)Brocato et al. (1996) (6)Chiosi & Vallenari (2007) (7)Crowl et al. (2001) (8)Kerber et al. (2007) (9)Mackey & Gilmore (2004) (10)Mighell et al. (1996) (11)Mighell et al. (1998b) (12)Olsen et al. (1998) (13)Testa et al. (1995) (14)van den Bergh (1981) (15)van den Bergh & Hagen (1968) (16)Walker (1992)

Table 6. This $\mathcal{M}_{(10\%)}$ limit is closely matched by composite cluster (age bin: $2-4.6$ Gyr) and surpassed by all others, ensuring a robust comparison between our measurements and model predictions.

3.3 The Old Cluster Population

Integrated JHK_S magnitudes were measured within the apertures of the optical photometry for all old clusters listed in Table B9. The photometry is presented in Table B10. We note that the data in the table are *measured* magnitudes, not corrected for reddening. A reddening correction *is* however applied when plotting the objects on the model grids in

Figures 3 – 16. Reddening values based on deep CMDs from the literature are used where available. For the rest of the sample, reddening estimates based on photometric information from the MCPS are applied.

In Figures 3 and 4 we show a comparison between the model predictions and reddening corrected colours for the 15 old Magellanic Cloud star clusters in our sample. The errorbars include uncertainties in the photometry, reddening correction, and an estimate of the error due to the statistical fluctuations within the field stellar population in the vicinity of each cluster. The most significant outliers, NGC 1928 and NGC 1939 (the two points in the lower left part of Figure 3), suffer from significant crowding due to their location in the LMC bar (see the remarks about NGC 1928 in Section 2.1). This likely affected their optical photometry measurements, which were retrieved from the literature[5]. However, the measured colours for most (other) clusters are generally in good agreement with the model predictions.

As mentioned in the previous section, it is possible that stochastic fluctuations in the number of (e.g., giant) stars will cause a spread of cluster colours at any given age and metallicity. In order to assess this effect, we estimate the stellar mass which contributes to our integrated magnitudes for each Magellanic Cloud cluster as follows. We use our extinction-corrected J- band magnitude (the 2MASS and Bessell & Brett photometric systems are closest in J and the 2MASS survey has its highest sensitivity in J), combined with the J band M/L ratios predicted by the Maraston (2005) models which assume a Kroupa (2001) IMF. These estimates of the stellar mass contributing to each observed colour are presented in Table B10. For comparison, we include mass estimates from McLaughlin & van der Marel (2005) which are determined from profile fitting (to determine the total cluster luminosity) combined with M/L_V ratios determined from SSP model fitting of each cluster (assuming the BC03 models with a Chabrier-disk IMF). While the two estimates are in reasonable agreement, our masses are systematically lower. We found that the main driver of this difference are the systematically lower total cluster luminosities compared to the values determined by McLaughlin & van der Marel (2005). This effect could be predicted since we do not extrapolate the cluster light outside of the aperture size used for the optical photometry. Secondary effects in the mass differences between the two works come from differences in the adopted ages and metallicities, and hence SSP M/L.

We divide the old cluster sample by metallicity into two subsamples, accumulating enough mass in each bin to render the effects of stochastic fluctuations negligible. Clusters with [Fe/H] < −1.71 are designated as "metal-poor" and shown as open blue circles on Figures 3 and 4), and those with [Fe/H]> −1.71 are referred to as "metal-rich" (depicted as open red diamonds). The mean magnitudes and colours cor-

[5] E.g., Elson & Fall (1985) derived S = 22 (Age ∼ 50 Myr) for NGC 1928 based on the integrated-light colours from van den Bergh (1981). This contradicts the results of Mackey & Gilmore (2004) based on high-resolution *HST/ACS* imaging, demonstrating clearly that the field contamination in the LMC bar region can significantly affect the integrated-light measurements if not properly accounted for.
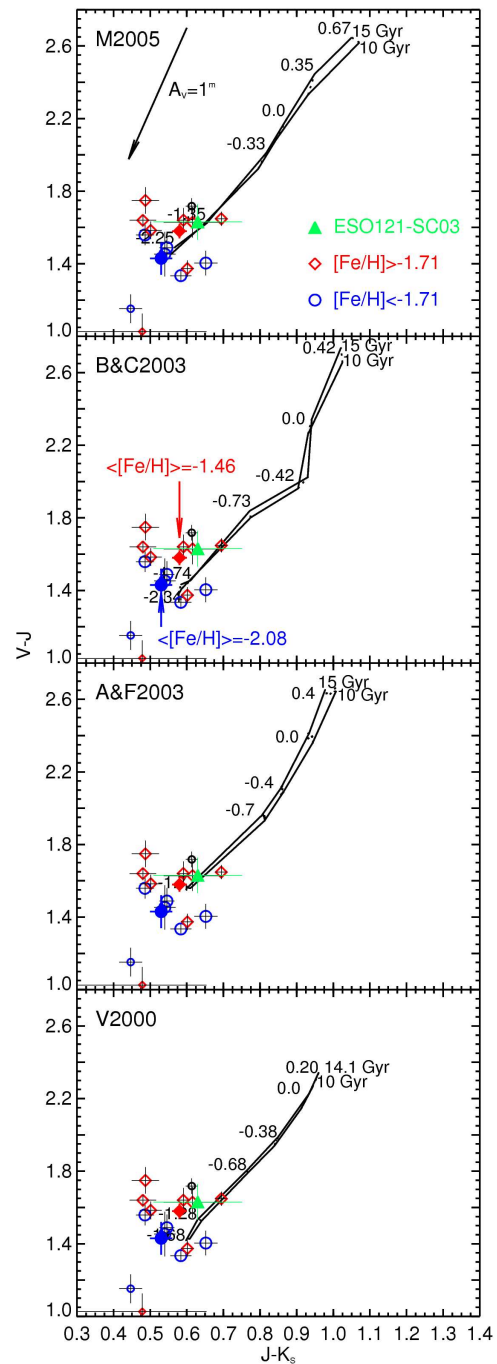
Figure 3. $(V-J)$ vs. $(J-K_S)$ colour-colour diagrams for the old clusters. Isochrones for 10 and 15 Gyr are plotted with solid lines and metallicity values are marked along them. The panels present the models of Maraston, Bruzual & Charlot, Anders & Fritze-v. Alvensleben and Vazdekis from top to bottom, respectively. The reddening vector is shown in the top panel. The two outliers are NGC 1928 (small red diamond) and NGC 1939 (small blue circle). NGC 1916 (small black circle) suffers from differential reddening (no age and metallicity available). The 9-Gyr-old cluster ESO121– SC03 is shown as a green triangle. Clusters with metallicities lower than the mean value for the sample are plotted as blue circles, the others are denoted with red diamonds. The mean colours for each of those sub-samples are shown as filled blue circle and red diamond respectively. The corresponding mean [Fe/H] values are shown in the second panel.

responding to the objects of the sub-sample are calculated from the sum of the fluxes of individual objects in each bin.

The metal-poor and metal-rich sub-samples have mean [Fe/H] values of -2.08 and -1.46 dex, respectively, and are presented along with the resulting metallicities (filled blue circle for the metal-poor clusters and filled red diamond for the metal-rich ones respectively). ESO121 – SC03, the ~ 9 Gyr cluster in the LMC, is also shown on these figures as a green triangle. The metal-rich and metal-poor globular cluster colours clearly separate in the optical-NIR colour-colour space, and generally follow the model predictions.

To provide a quantitative measure (and a summary) of the performance of the different models in terms of fitting the average colours of the various subsamples, we compiled the relevant information in Table 6 (for *all* age groups). The mean colours of the composite clusters are listed there along with the interpolated model predictions for the ages and metallicities corresponding to the composite points (using linear interpolation between adjacent model isochrones and iso-metallicity grid lines), as well as the measured colour differences between the data and the model predictions (we will hereafter refer to these colour differences as "absolute colour residuals"). In Table 6 we also present the inferred ages and metallicities of the composite clusters according to the models. In some cases it is not possible to derive reliable stellar population properties due to insufficient coverage of the model grids (those are left blank in the table). For the old metal-rich cluster sub-sample ($<$[Fe/H]$>= -1.46$) *all* models (Vazdekis 1999; Bruzual & Charlot 2003; Maraston 2005) infer ages exceeding the corresponding oldest model isochrones. Maraston models with BHB are in a good agreement with the mean composite cluster ages for the entire old cluster sample and the metal-poor ($<$[Fe/H]$>= -2.08$) sub-sample, although the inferred metallicities are a little lower than the mean values for each composite point.

Inspection of Table 6 shows that the models of Maraston (2005) (with BHB) provide the best overall match to the observations of old clusters, especially in terms of estimating their ages, while the Bruzual & Charlot (2003) models formally do the best job of estimating SSP metallicities.

3.4   The 2 Gyr $\leqslant$ Age < 10 Gyr Cluster Population

Nine LMC and six SMC clusters with adequate age and metallicity measurements were selected in this age interval. Information on the cluster ages, metallicities, and masses are compiled in Tables B9 and B10. A comparison between our photometry and the model tracks in $V-J$ vs. $J-K_S$ and $B-J$ vs. $J-K_S$ colour-colour diagrams are shown in Figures 5 and 6, respectively. We further divide the $2-10$ Gyr sample into two subsamples, with ages older than and younger than 4.6 Gyr. When compared with the Maraston (2005) models, these show that generally the younger subsample agrees with the predicted location of the 2 Gyr model, and that the older bin also falls in the expected region of colour-colour space.

Because this bin includes a large range of ages and some of the individual clusters have stellar mass estimates lower than $\mathcal{M}_{LLL}$ (see Section 3.2), one can expect some scatter among the individual measurements with respect to the model predictions, which is indeed observed. Most of our mass estimates in this age bin are systematically lower than

those of McLaughlin & van der Marel (2005) (see § 3.3 for possible explanation). The composite clusters representing the entire sample in this age range and the metal-poor older subpopulation (4.6 Gyr $\leqslant$ Age < 10 Gyr) both accumulate masses exceeding $\mathcal{M}_{(10\%)}$, so that the composite colours ought to yield meaningful comparisons to the SSP model predictions. Unfortunately this is not quite the case for the younger metal-rich subpopulation (2 Gyr $\leqslant$ Age < 4.6 Gyr). These clusters do however, exceed $\mathcal{M}_{LLL}$ by a factor of ~ 10, so while we might expect some bias in the colors it is certainly worth presenting information in this age range in Table 6. We point out that these results must be treated with some caution (also noted in the table). Reliable ages and metallicities are needed for more clusters in this particular age interval in order to provide more accurate comparison between model predictions and observed properties of the stellar populations.

All four sets of models reproduce the mass-weighted average colours reasonably well in terms of quantitative colour differences (see Table 6). Ages and metallicities inferred by *all* SSP models for the three composite clusters in this age interval are also listed in the table. There is some degeneracy present in the Maraston (2005) models in this regime due to the intersection of the 10 Gyr and 4 Gyr isochrones in colour-colour space. Taking this into account, it is not possible to infer a single value for the stellar population's age or metallicity. Stellar population properties measured with respect to different Maraston isochrones are listed in Table 6. There is good agreement between the mean ages of the composite clusters and the ages infered by the model, but the corresponding metallicities are typically lower. Generally all models provide consistent stellar population properties between both colour-colour diagrams typically showing somewhat lower ages and higher metallicities. In some cases differences are observed in the inferred properties of the stellar populations for some sub-samples in this age interval (see Table 6), when predictions are based on $(V-J)$ vs. $(J-K_S)$ vs. the $(B-J)$ vs. $(J-K_S)$ colour-colour diagrams. Note that all models (except Maraston) infer super-solar metallicities for the (2 Gyr $\leqslant$ Age < 4.6 Gyr) subpopulation. Further investigation is needed to determine whether it is a model ingredient or assumption that is responsible for the mismatch, or whether this mismatch occurs due to insufficient mass accumulated in the age bin.

Overall the Maraston (2005) models provide the best inference about the properties of the stellar populations in this age range.

3.5   The 1 Gyr $\leqslant$ Age < 2 Gyr Cluster Population

Eleven LMC and two SMC clusters with adequate age and metallicity measurements from CMDs and/or spectroscopy of individual giant stars were selected in this age interval (see Tables B9 and B10). Our photometry and the model tracks in $V-J$ vs. $J-K_S$ and $B-J$ vs. $J-K_S$ colour-colour space are compared in Figures 7 and 8. This age interval covers a period after the "AGB phase transition", i.e., the onset of the AGB phase and coincides with the development of the RGB. Therefore a significant impact on the light output in the NIR (especially in the K-band) is expected. Hence it is important to maximize the number of objects so as to accumulate enough mass and decrease the effects of the

stochastic fluctuations in the stellar population. We added five clusters to our composite based on their recalibrated '"S-parameter" values (the S-parameter is an age indicator based on integrated $U - B$ and $B - V$ colours, (see Elson & Fall 1985; Girardi et al. 1995)). Our recalibration of the S-parameter based on recent cluster age determinations is described in detail in Appendix A. The total mass of the composite cluster with ages between 1 and 2 Gyr is $\mathcal{M}_{\rm tot} = 3.6 \times 10^5 \mathcal{M}_\odot$, which exceeds $\mathcal{M}_{(10\%)}$.

Overall, the colours of clusters in this age range agree reasonably well with the SSP model predictions. Maraston models most accurately reproduce the age of the composite cluster, although it indicates too low a metallicity. The latter is the reason why the Maraston model has the largest colour residual for this age range in Table 6. The performance of the other three models in this age range are similar to one another: They all indicate an age that is somewhat too young and a metallicity that is somewhat too high, but the absolute colour residuals are smaller than that of the Maraston model. Quantitatively, the Bruzual & Charlot (2003) model comes out best in this age range in terms of absolute colour residuals.

3.6 The 200 Myr ⩽ Age < 1 Gyr Cluster Population

In this age range, we identified only three clusters (2 in the LMC and 1 in the SMC) with reliable age and metallicity estimates based on currently available deep CMDs (See Table B9). As in the previous age bin, we added other clusters based on our recalibration of the S parameter (see Appendix A), resulting in the addition of 5 objects to this age bin. Model tracks in the $V - J$ vs. $J - K_S$ and $B - J$ vs. $J - K_S$ colour-colour space are presented along with our photometry results in Figures 9 and 10. The total mass of the composite cluster of this age range is $\mathcal{M}_{\rm tot} = 1.1 \times 10^5 \mathcal{M}_\odot$, as listed in Table 6. Unfortunately this barely exceeds $\mathcal{M}_{(10\%)}$. More reliable age and metallicity estimates are needed for Magellanic Cloud star clusters in this age interval to be able to provide calibration data that could be crucial to improve the treatment of the AGB phase and perform further tests of the models. Overall, the Bruzual & Charlot (2003) and Maraston (2005) models perform best in this age range. The models of Bruzual & Charlot (2003) and Maraston (2005) yield similar metallicity estimates, which are *too low*. Bruzual & Charlot (2003) overestimates slightly the mean age of the composite cluster, Maraston (2005) infer age that is younger. The Bruzual & Charlot (2003) models have the smallest colour residuals in this age range.

3.7 The Complete Sample

In Figure 11 we present the entire cluster sample, from 200 Myr to 12 Gyr, studied in the previous sections. One of the main attractions for using a combination of reddening-corrected optical and NIR integrated colours is that it is supposed to break the age-metallicity degeneracy. Can it actually do this? First, we note the important caveat that in the Magellanic Clouds, the typical cluster mass increases with age. This is partly a statistical effect (e.g., Hunter et al. 2003; Whitmore et al. 2007), due to the fact that the younger

age bins cover shorter times, and fewer clusters formed originally in these shorter time intervals, leading statistically to a somewhat lower typical cluster mass at younger ages. The large spread in intrinsic colours among young clusters is due in part to the low masses of these clusters which naturally causes stochastic fluctuations in the numbers of massive IR-luminous stars. Another contributor to the larger spread in colours is the fact that the IR-luminous stars in these objects (i.e., the AGB stars) have shorter lifetimes and higher luminosities relative to their counterparts at older ages (i.e., RGB stars) . Despite these effects, we find that overall, clusters in different age bins do in fact, appear to occupy different regions of colour-colour space, although with a relatively large spread. The solid points reflect the mean colour for each age bin discussed in the previous sections, most of which have accumulated masses larger than $\mathcal{M}_{(10\%)}$. The solid points in Figure 11 suggest that the following conclusions can be safely drawn for massive SSPs based solely on the combination of $B - J$ and $J - K$ (or $V - J$ and $J - K$) colours: *(i)* ages older than roughly 9 Gyr can be separated from those younger than ≈ 5 Gyr; *(ii)* ages of ≈ 2 Gyr can be adequately separated from those older than ≈ 5 Gyr ; and *(iii)* finally, ages younger than 1 Gyr separate nicely from those older than 1 Gyr.
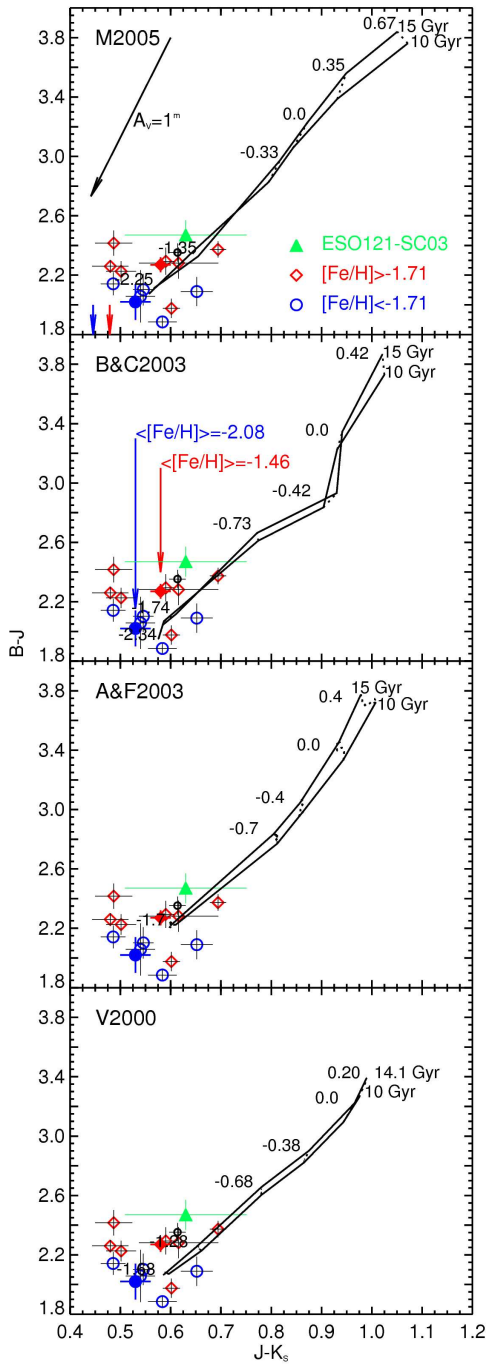
Figure 4. $(B - J)$ vs. $(J - K_S)$ colour-colour diagrams for the old clusters. As in Figure 3 two different isochrones are plotted and metallicity values are marked. The panels are organized in the same order, with an extinction vector shown in the top panel. The two clusters NGC 1928 and NGC 1939, fall outside of the diagrams, and the directions towards them are marked with red and blue arrow respectively. NGC 1916 is shown as a small black circle.
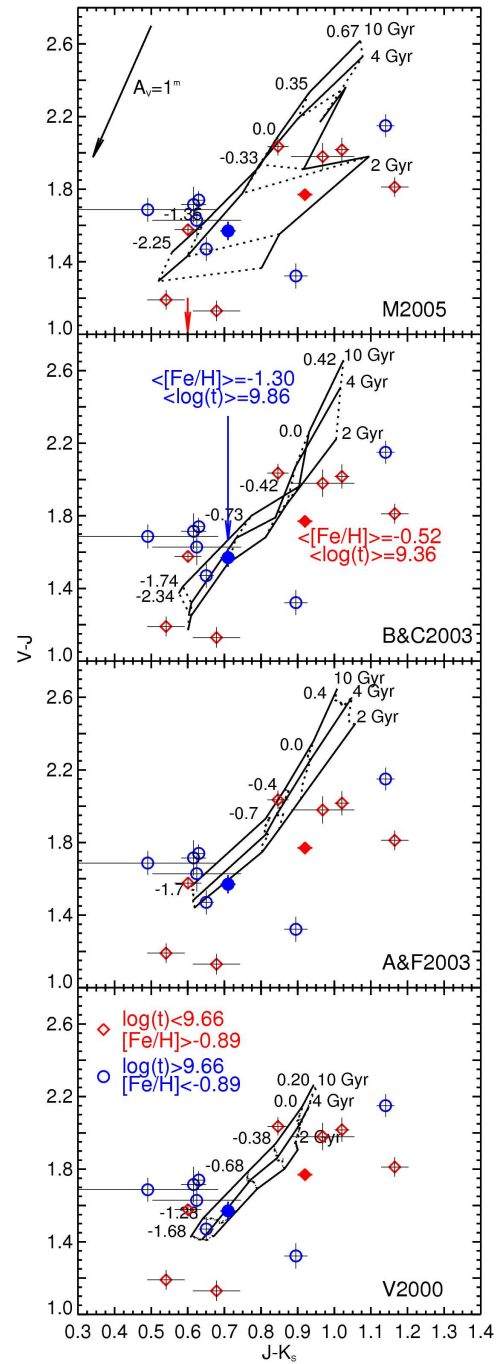
Figure 5. $(V - J)$ vs. $(J - K_S)$ colour-colour diagrams for the clusters between 2 and 10 Gyr. The isochrones for three different ages are plotted with solid lines and metallicity values are marked along the model tracks for 10 Gyr. Black dotted lines stand for equal metallicity. The four panels show four SSP models as in Figure 3. A reddening vector for $A_V = 1^m$ is shown in the top panel. A legend to the individual symbols is provided in the bottom panel. The composite sub-samples are marked with filled symbols, along with their errors (colour-coded solid lines). The mean age and metallicity for each sub-sample are indicated in the second panel. The red arrow points to the position of **Hodge 4**, falling outside the boundaries of the plotted colour-colour space.
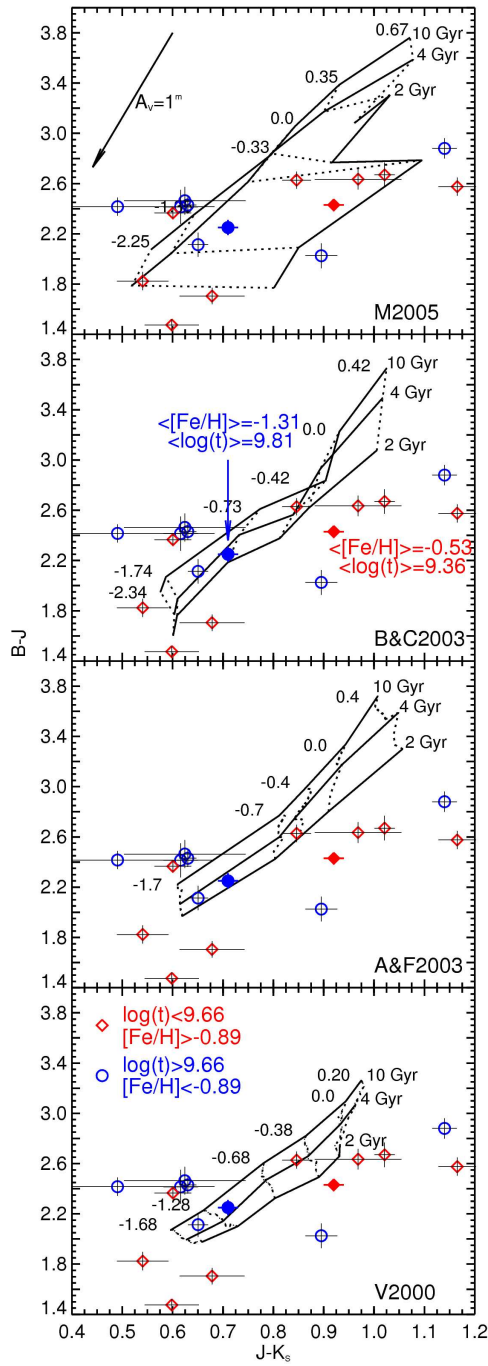
Figure 6. As Figure5, but for $(B - J)$ vs. $(J - K_S)$.
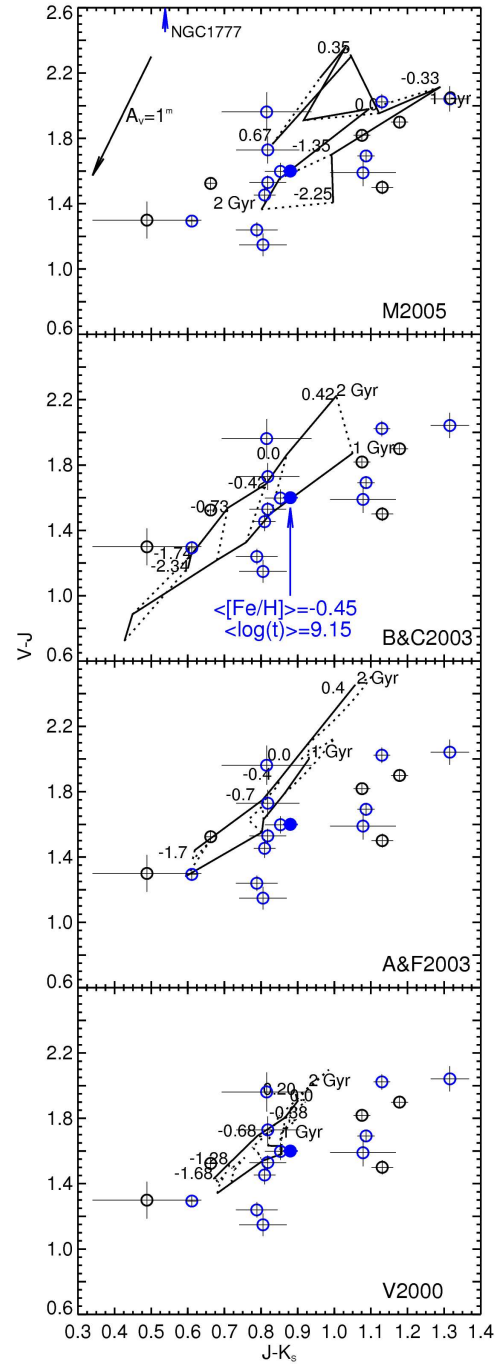
Figure 7. $(V - J)$ vs. $(J - K_S)$ colour-colour diagrams for the clusters between 1 and 2 Gyr. Isochrones for the different ages are plotted with solid lines and metallicity values are marked along the 2 Gyr isochrone. The four panels show four SSP models as in Figures 3–6. The blue circles represent clusters with reliable age and metallicity estimates retrieved from the literature, while black circles denote the objects added to the sample on the basis of our S-parameter recalibration (see Appendix A). The composite cluster is marked by a filled circle, along with its error (solid blue lines). The mean age and metallicity are indicated in the second panel.
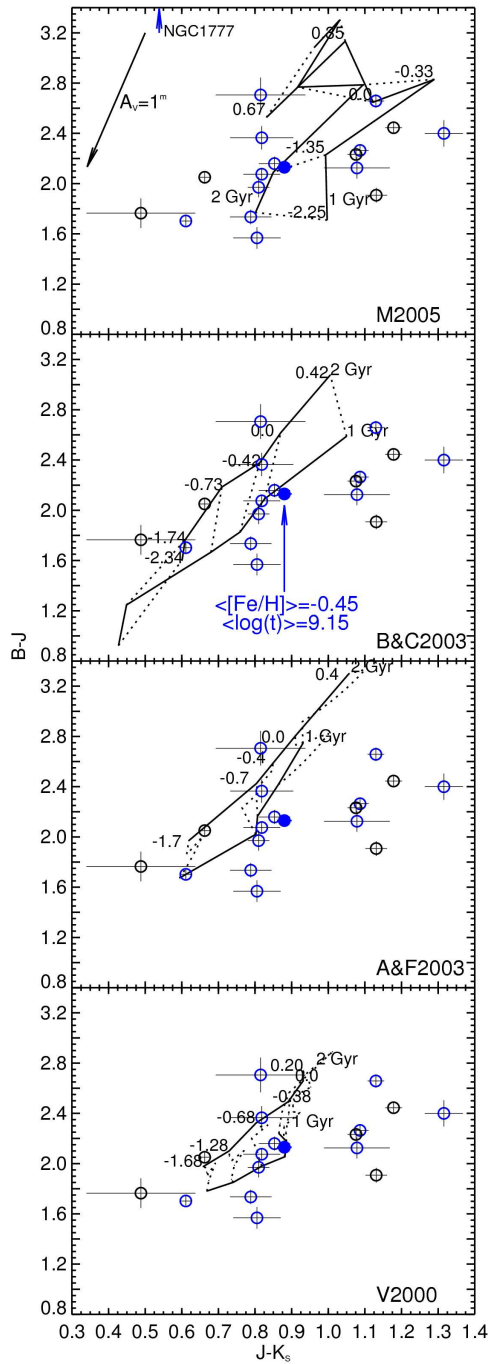
Figure 8. Same as Figure 7, but for $(B - J)$ vs. $(J - K_S)$
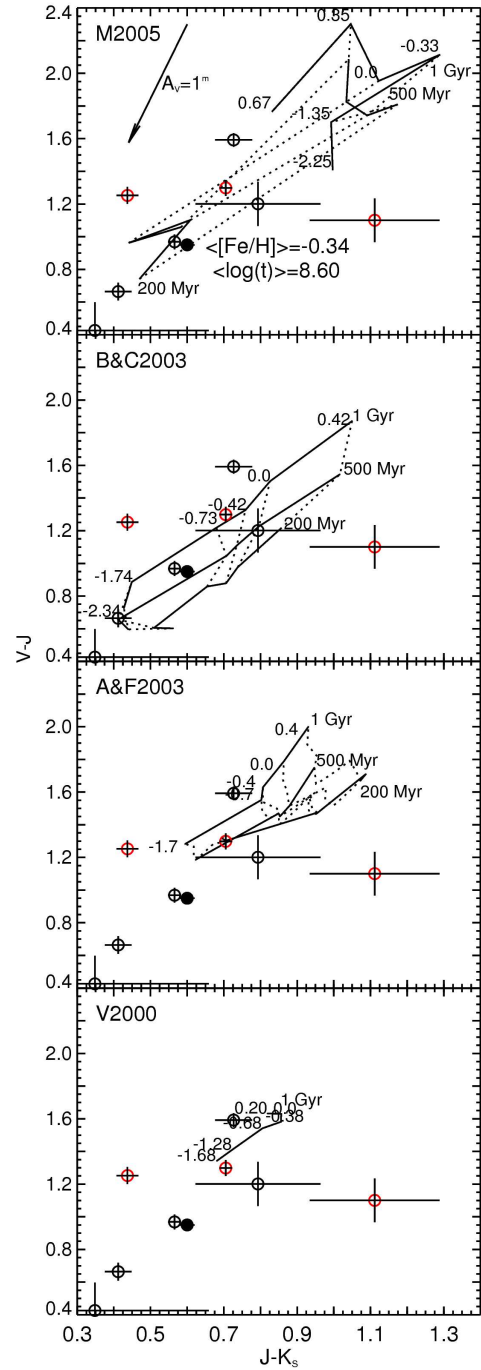

Figure 9. $(V - J)$ vs. $(J - K_S)$ colour-colour diagrams for the clusters between 200 Myr and 1 Gyr. The information (order of presentation of the models, extinction) is shown as in the figures for the other age bins. Three isochrones are plotted for each model (except for V2000 whose models do not include colour information for ages younger than 1 Gyr). The dotted lines show equal metallicities, and their values are marked along the 1 Gyr isochrone. The red circles represent clusters with reliable age and metallicity estimates retrieved from the literature, black circles denotes the objects added to the sample on the basis of our S-parameter re-calibration. The composite cluster is marked with filled black symbol, along with its error (solid lines). Its mean age and metallicity are indicated at the top panel.
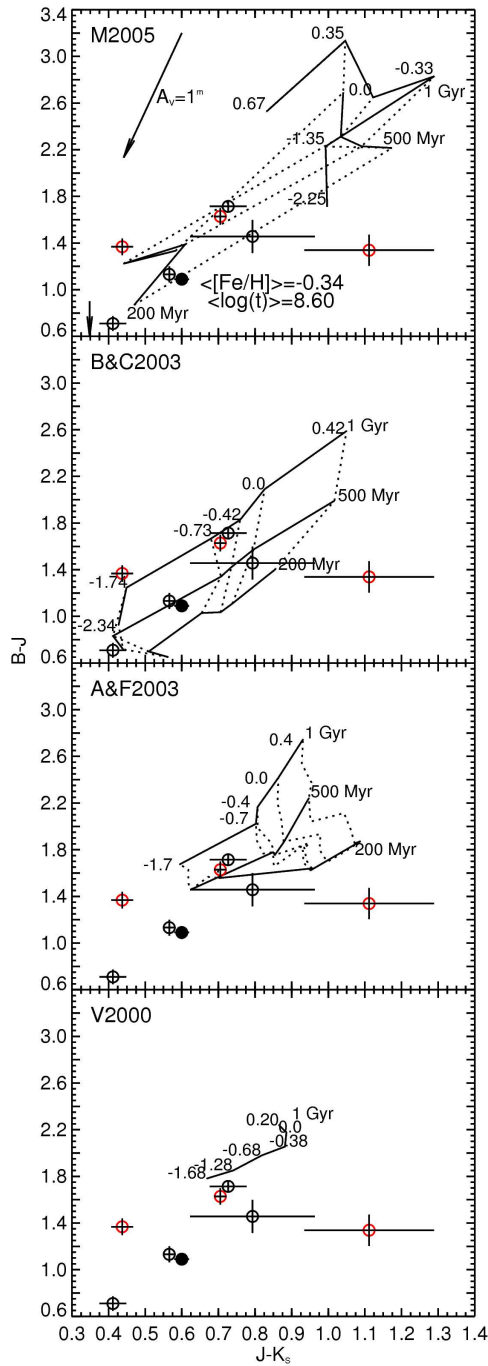
Figure 10. $(B-J)$ vs. $(J-K_S)$ colour-colour diagrams for the clusters between 200 Myr and 1 Gyr. Generally the notes are the same as for the 200 Myr - 1 Gyr $(V-J)$ vs. $(J-K_S)$ colour-colour diagram. The only difference is the black arrow in the top panel, pointing toward the position of NGC2156, which in this case is located out of the colour boundaries of the panels.
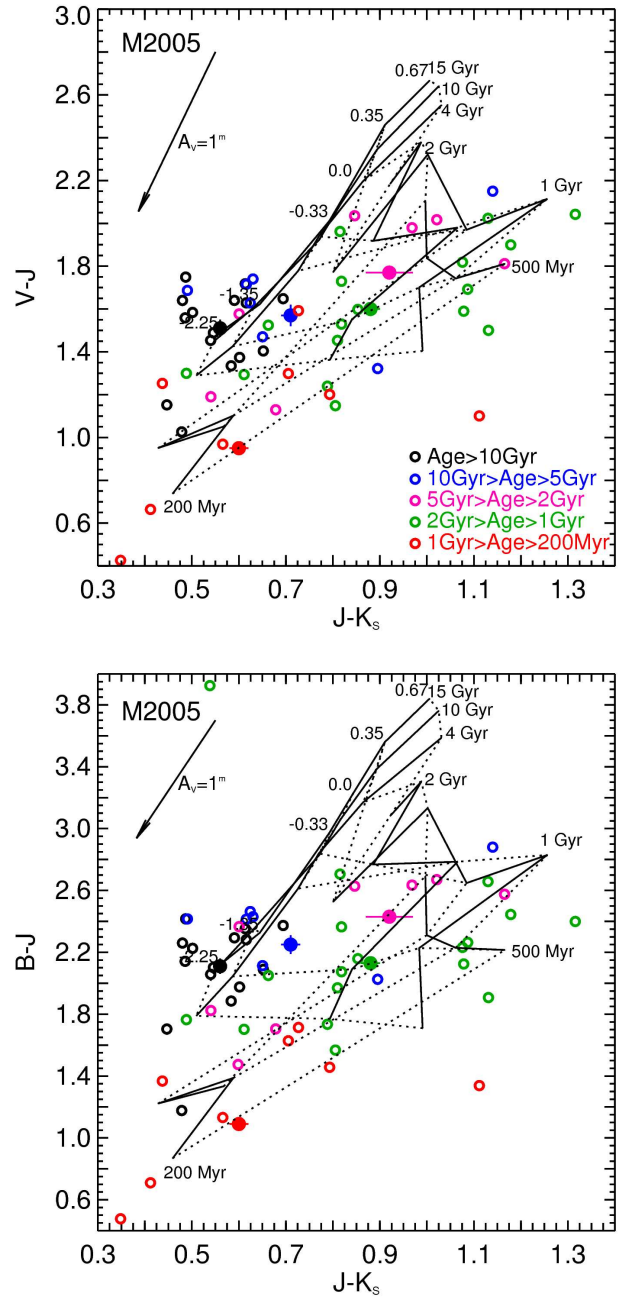

Figure 11. Data of all 54 clusters from our test sample on top of the grid of Maraston 2005 models in the $(V-J)$ vs. $(J-K_S)$ and $(B-J)$ vs. $(J-K_S)$ colour-colour space. The individual points are colour-coded according to the age of the object (see the legend). The mean colours for each age bin are presented with filled circles. The error bars show the corresponding error of the mean colour.

Table 6. Information about the composite clusters and model performance.

COMPOSITE COLOURS (CC) $(B-J)_0$ $\sigma_{(B-J)_0}$	$(V-J)_0$ $\sigma_{(V-J)_0}$	$(J-K_S)_0$ $\sigma_{(J-K_S)_0}$	MODEL PREDICTIONS (MP) Mod.[a]	$(B-J)$	$(V-J)$	$(J-K_S)$	CC – MP $\Delta(B-J)$	$\Delta(V-J)$	$\Delta(J-K_S)$	DISTANCE R_B	R_V	POPULATION PROPERTIES $(B-J)$ vs. $(J-K_s)$ $log(\tau)$	[Fe/H]	$(V-J)$ vs. $(J-K_s)$ $log(\tau)$	[Fe/H]
(1)	(2)	(3)	(4)	(5)	(6)	(7)	(8)	(9)	(10)	(11)	(12)	(13)	(14)	(15)	(16)
Old globular clusters (Ages $\geqslant$ 10 Gyr): 14 objects, $< [Fe/H] >= -1.71$, $log(\mathcal{M}_{tot}) = 6.47^{+0.09}_{-0.11}$, $log(\mathcal{M}_{LLL}) = 4.04$, $log(\mathcal{M}_{(10\%)}) = 5.22$															
2.11	1.51	0.56	**AF03**	2.24	1.57	0.60	−0.13	−0.06	−0.04	4.77	4.27				
0.05	0.04	0.01	**BC03**	2.11	1.44	0.60	0.00	+0.07	−0.04	4.00	4.37	> 10.30	−1.74	> 10.30	−1.83
			M05	2.20	1.53	0.60	−0.09	−0.02	−0.04	4.39	4.03	10.18	−2.25	10.18	~ -2.25
Old globular clusters (Ages $\geqslant$ 10 Gyr), [Fe/H] < -1.71: 5 objects*, $< [Fe/H] >= -2.08$, $log(\mathcal{M}_{tot}) = 6.01^{+0.11}_{-0.14}$, $log(\mathcal{M}_{LLL}) = 4.00$, $log(\mathcal{M}_{(10\%)}) = 5.18$															
2.02	1.43	0.53	**BC03**	2.03	1.42	0.59	−0.01	+0.01	−0.06	2.00	2.00	> 10.30	−2.10	> 10.30	−2.34
0.12	0.09	0.03	**M05**	2.12	1.49	0.57	−0.10	−0.06	−0.04	1.57	1.49	~ 10.10	< −2.25	10.10	< −2.25
Old globular clusters (Ages $\geqslant$ 10 Gyr), [Fe/H] $\geqslant -1.71$: 7 objects**, $< [Fe/H] >= -1.46$, $log(\mathcal{M}_{tot}) = 6.24^{+0.08}_{-0.10}$, $log(\mathcal{M}_{LLL}) = 4.07$, $log(\mathcal{M}_{(10\%)}) = 5.26$															
2.27	1.61	0.58	**V00**	2.16	1.47	0.61	+0.11	+0.14	−0.03	2.66	3.81	> 10.25	−1.50	> 10.25	−1.28
0.05	0.04	0.02	**AF03**	2.29	1.60	0.62	−0.02	+0.01	−0.04	2.04	2.02	> 10.18	< −1.70	> 10.18	< −1.70
			BC03	2.19	1.53	0.68	+0.08	+0.08	−0.10	5.25	5.39	> 10.30	−1.42	> 10.30	−1.19
			M05	2.30	1.59	0.63	−0.03	+0.02	−0.05	2.57	2.55	> 10.18	−1.66	~ 10.18	−1.65
10 Gyr > Age $\geqslant$ 2 Gyr sample: 15 objects, $< [Fe/H] >= -0.89$, $< log(t) >= 9.66$, $log(\mathcal{M}_{tot}) = 5.68^{+0.10}_{-0.13}$, $log(\mathcal{M}_{LLL}) = 4.19$, $log(\mathcal{M}_{(10\%)}) = 5.37$															
2.34	1.67	0.83	**V00**	2.28	1.61	0.74	+0.06	+0.06	+0.09	9.12	9.22	9.30	−0.54	9.30	−0.68
0.04	0.03	0.01	**AF03**	2.36	1.68	0.73	−0.02	−0.01	+0.10	10.01	10.01	9.18	−0.28	9.18	−0.70
			BC03	2.19	1.53	0.68	+0.15	+0.14	+0.15	15.46	15.71	9.22	−0.12	9.30	−0.42
			M05[b]	2.13	1.48	0.61	+0.21	+0.19	+0.22	22.62	22.89	9.71	−0.65	9.79	−0.61
												9.42	−0.80	9.54	−0.78
10 Gyr > Age $\geqslant$ 4.6 Gyr sample, [Fe/H] < -0.88: 7 objects, $< [Fe/H] >= -1.30$, $< log(t) >= 9.86$, $log(\mathcal{M}_{tot}) = 5.55^{+0.11}_{-0.14}$, $log(\mathcal{M}_{LLL}) = 4.11$, $log(\mathcal{M}_{(10\%)}) = 5.22$															
2.25	1.57	0.71	**V00**	2.18	1.52	0.66	+0.07	+0.05	+0.05	2.76	2.69	9.74	−1.05	9.48	−1.08
0.06	0.05	0.02	**AF03**	2.26	1.59	0.65	−0.01	−0.02	+0.06	3.01	3.03	9.48	−0.96	9.30	−0.96
			BC03	2.08	1.43	0.62	+0.17	+0.14	+0.09	5.32	5.30	9.43	−0.73	9.38	−0.73
			M05[b]	2.23	1.53	0.62	+0.02	+0.04	+0.09	4.51	4.57	9.91	−0.74	9.90	−0.75
												9.52	−1.35	9.51	−1.35
4.6 Gyr > Age $\geqslant$ 2 Gyr sample, [Fe/H] $\geqslant -0.88$: 8 objects, $< [Fe/H] >= -0.52$, $< log(t) >= 9.36$, $log(\mathcal{M}_{tot}) = 5.08^{+0.08}_{-0.09}$, $log(\mathcal{M}_{LLL}) = 3.98$, $log(\mathcal{M}_{(10\%)}) = 5.28$															
2.43	1.77	0.92	**V00**[c]	2.31	1.67	0.76	+0.12	+0.10	+0.16	8.54	8.67	9.15	0.20		
0.04	0.03	0.02	**AF03**	2.56	1.84	0.83	−0.13	−0.07	+0.09	5.86	5.07	8.89	0.40	8.84	0.00
			BC03	2.40	1.66	0.77	+0.03	+0.11	+0.15	7.54	8.35	9.21	0.21	9.17	0.20
			M05[d]	2.44	1.74	0.90	−0.01	+0.03	+0.02	1.03	1.41	9.50	−0.59	9.60	−0.65
												9.37	−0.61	9.38	−0.57
														8.62	0.35
2 Gyr > Age $\geqslant$ 1 Gyr sample: 17 objects***, $< [Fe/H] >= -0.45$, $< log(t) >= 9.15$, $log(\mathcal{M}_{tot}) = 5.55 \pm 0.06$, $log(\mathcal{M}_{LLL}) = 3.75$, $log(\mathcal{M}_{(10\%)}) = 5.11$															
2.13	1.60	0.88	**V00**	2.35	1.74	0.86	−0.22	−0.14	+0.02	7.40	7.07	9.00	−0.21		
0.03	0.02	0.02	**AF03**	2.40	1.75	0.81	−0.27	−0.15	+0.07	9.06	8.28	8.88	0.13	8.80	0.05
			BC03	2.24	1.61	0.83	−0.11	−0.01	+0.05	4.44	2.55	8.77	0.15	9.00	0.15
			M05[e]	2.64	1.94	1.14	−0.51	−0.34	−0.26	21.40	21.40	9.26	−1.35	9.26	−1.35
												8.52	0.24	8.59	0.00

Notes to Table 6: See page 18.

Table 6. Information about the composite clusters and model performance.

COMPOSITE COLOURS (CC)			MODEL PREDICTIONS (MP)				CC – MP			DISTANCE		POPULATION PROPERTIES			
$(B-J)_0$	$(V-J)_0$	$(J-K_S)_0$										$(B-J)$ vs. $(J-K_s)$		$(V-J)$ vs. $(J-K_s)$	
$\sigma_{(B-J)_0}$	$\sigma_{(V-J)_0}$	$\sigma_{(J-K_S)_0}$	**Mod.**[a]	$(B-J)$	$(V-J)$	$(J-K_S)$	$\Delta(B-J)$	$\Delta(V-J)$	$\Delta(J-K_S)$	R_B	R_V	$log(\tau)$	[Fe/H]	$log(\tau)$	[Fe/H]
(1)	(2)	(3)	(4)	(5)	(6)	(7)	(8)	(9)	(10)	(11)	(12)	(13)	(14)	(15)	(16)
1 Gyr $>$ Age $\geqslant$ 200 Myr sample: 8 objects, $<[Fe/H]>=-0.34$, $<log(t)>=8.60$, $log(\mathcal{M}_{tot})=5.04^{+0.05}_{-0.06}$, $log(\mathcal{M}_{LLL})=3.60$, $log(\mathcal{M}_{(10\%)})=5.05$															
1.09	0.95	0.60	**AF03**	1.85	1.59	0.95	−0.76	−0.64	−0.35	25.83	27.59				
0.04	0.03	0.02	**BC03**	1.24	1.01	0.72	−0.15	−0.06	−0.12	7.08	6.33	8.64	−0.89	8.78	−0.89
			M05	2.10	1.66	1.01	−1.01	−0.71	−0.41	32.52	31.31	8.40	−1.35	8.41	−1.35

Notes to Table 6: Columns (1) – (3) list the weighted mean colours of the composite clusters, along with their corresponding errors. The number of clusters combined in each composite, their mean ages and metallicities plus the total accumulated mass is shown on the line above the colours. Masses associated with the Lowest Luminosity Limit $\mathcal{M}_{LLL}$ and 10% accuracy limit $\mathcal{M}_{(10\%)}$ are presented for comparison. Columns (4) – (12) show the results of the model and data comparison. Column (4) denotes the model: **M05** stands for Maraston (2005), **BC03** for Bruzual & Charlot (2003), **AF03** for Anders & Fritze-v. Alvensleben (2003), and **V00** for Vazdekis (1999). Columns (5) through (7) give the interpolated colours predicted by the models for the mean ages and metallicities of the composite clusters. The corresponding differences in colour space (data minus model predictions) are given in columns (8) – (10). Finally columns (11) and (12) give a distance between the positions predicted by the models and the composite cluster locations calculated as $R_X = \sqrt{(\Delta C1/\sigma_{C1})^2 + (\Delta C2/\sigma_{C2})^2}$, where ΔCi is the corresponding colour difference and σ_{Ci} is the uncertainty of the mean colour of the composite cluster. R_V stands for the distance in the $(J-K_S)$ vs. $(V-J)$ colour-colour space, and R_B for the $(J-K_S)$ vs. $(B-J)$ distance. The composite colours and corresponding uncertainties are calculated by summing the flux of the clusters in the corresponding subpopulation. The cumulative mass in each composite cluster is calculated as the sum of the individual cluster masses.

The following objects were excluded from the corresponding composite clusters (marked with asterisks in the table) due to possible foreground/background contamination and/or small aperture diameters of the optical photometry.

* NGC1939 is excluded from the mean.

** NGC1928 is excluded from the mean.

*** NGC1777 is excluded from the mean.

(a) We did not extrapolate in cases when the ages and metallicities of the composite clusters were out of the parameter space covered by the models. This is affecting the comparisons in the cases of "old" globular clusters and for the youngest age bin. A rough estimate of the model performance in these cases can be obtained from the figures, showing the data for the corresponding age bins (see Fig.3, 4, 7 – 10).

(b) In this case there is degeneracy in the Maraston (2005) model predictions, in sense that 10 and 4 Gyr isochrones are overlapping in the colour-colour space. The composite-cluster ages and metallicities inferred by the models with respect to the 4 Gyr isochrone are listed in the table on the row below the model predictions for the 10 Gyr isochrone.

(c) Some degeneracy is present for the 1 Gyr isochrone of Vazdekis (1999), especially in the $(V-J)$ vs. $(J-K_S)$ colour-colour space.

(d) The properties of the composite cluster for the younger sub-sample in the 10 Gyr $>$ Age $\geqslant$ 2 Gyr age bin are derived taking into account the degeneracy due to the intercept of the 10 and 4 Gyr isochrones. In the $(V-J)$ vs. $(J-K_S)$ colour-colour diagram, the corresponding data also falls in the parameter space covered by the clusters with ages between 200 Myr and 500 Myr. Ages and metallicities inferred by the **M05** model for each of these cases are listed in columns (13) – (16) of the table: the first line (with respect to the 10 Gyr isochrone), second (4 Gyr isochrone) and third (200 – 500 Myr case).

(e) Colour degeneracy between $1 - 2$ Gyr and 200 Myr – 1 Gyr **M05** models. The inferred stellar population properties are listed in the first ($1 - 2$ Gyr case) and second (200 Myr – 1 Gyr) line of columns (13) – (16) in the table.

3.8   Age-Colour Comparison

In this section we compare the observed cluster colours and
the mean sub-sample colours with model predictions as a
function of age. Integrated-light colour age evolution is a
basic SSP model prediction and Magellanic Cloud clusters
are the only objects that allow these predictions to be tested
for intermediate ages. This information is shown here to pro-
vide feedback to model builders by identifying ages at which
the discrepancies occur, hence pointing to the responsible
stages of stellar evolution and model ingredients that need
further attention and refinement. Results for several optical
and NIR colours are presented in Figures 12 − 16.

The $(B-V)$ colour is presented in Figure 12. The clus-
ters in our test sample comply with the LLL criterion (see
Section 3.2) in the optical and the distribution of the indi-
vidual points around the model tracks is reasonably tight.
There is good agreement between the properties of the com-
posite clusters and the model predictions. The correlation
between age and optical colours is well illustrated in this
figure as well as the relatively poor metallicity resolution.

Figures 13 – 16 present combinations of optical-NIR
colours (except for $(J - K_S)$ on Figure 16). These illus-
trate that the majority of the models tested in the present
paper show a "bump" towards redder colors between 1 and
2 Gyr, which is likely due to the development of the RGB.
The exception appears to be the Maraston (2005) model.
However, the latter shows a relatively pronounced effect of
the AGB phase transition (starting at a few hundred Myr).
Note the steep increase of the predicted colours, due to the
increased flux in the NIR passbands. This increased AGB
contribution in the Maraston models may be a reason why
the development of the RGB is not as visually prominent as
in the other models.

Also note that the colors of the composite and the in-
dividual clusters in the youngest age bin are in much better
agreement with the predictions of the Maraston (2005) mod-
els if age estimates from Girardi et al. are used (these are
the ages which were available at the time). Our recalibra-
tion of the S-parameter described in Appendix A shifts the
ages in this interval to older values by 0.2 dex, introduc-
ing a slight discrepancy with the Maraston (2005) models,
but in good agreement with the Bruzual & Charlot models.
In other words, the models of Maraston seem to reflect our
knowledge of the ages of Magellanic Cloud clusters prior to
2005. Our study may be used to make appropriate updates
to the models.

4   CONCLUDING REMARKS

We have presented new integrated JHK_s 2MASS photome-
try for 9 Magellanic Cloud clusters, bringing our total sam-
ple (when combined with the results of Paper I) to 54 clus-
ters with reliable ages ⩾200 Myr. In addition, we compile
integrated-light B and V photometric measurements, ex-
tinction estimates, and a database of reliable age and metal-
licity determinations (mostly recent results) from the liter-
ature for our sample clusters. We divide the clusters into
different age (e.g., ⩾ 10 Gyr, 3−9 Gyr, 3−4 Gyr, 1−2 Gyr,
and 200 Myr−1 Gyr) and metallicity (when possible), and
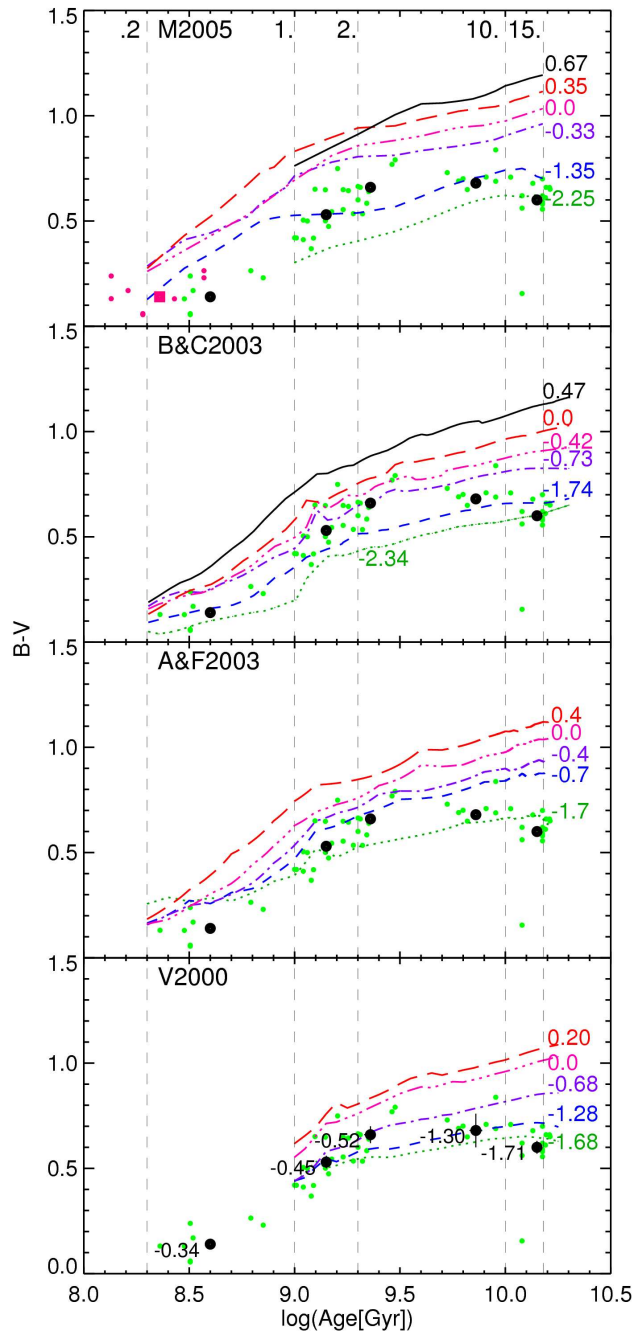quantify the observed spread in the intrinsic cluster colours

Figure 12. $(B - V)$ colour predicted by the models of Maraston
2005, Bruzual & Charlot 2003, Anders & Fritze 2003 and Vazdekis
1999 (from top to bottom) as a function of age for different metal-
licities (labeled at the end of the colour-coded lines). Vertical
dashed lines depict the boundaries of the age bins adopted in
the present study. The reddening-corrected colours of the indi-
vidual clusters from our sample are represented with small green
dots. Solid black points show the mean colours of the sub sam-
ples, labeled by corresponding mean metallicities. The positions
of the clusters in the youngest age bin when taking into account
the ages derived by the S parameter calibration of Girardi et al.
(1995) are shown as magenta dots on the top panel (the magenta
square stands for the mean colour in this case). The prominent
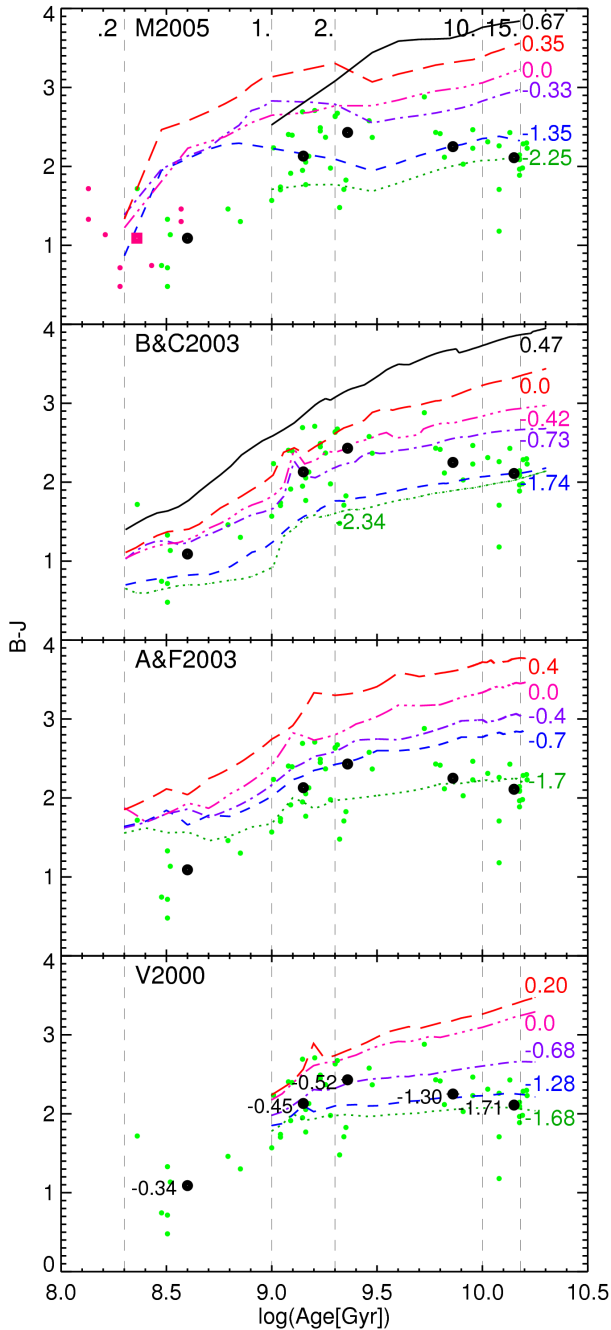outlier in the oldest age bin is NGC 1928.

Figure 13. The same as Figure 12, but for $(B - J)$ colour.

Figure 14. The same as Figure 12, but for $(V - J)$ colour.

in these ranges. Care was taken to account for the spread of the observational data around the model predictions due to the stochastic fluctuations in the stellar populations of the clusters. The smallest spread in intrinsic colours is found for clusters with ages $\gtrsim 10$ Gyr, the colours of which are well-reproduced by all four sets of SSP model predictions. The systematic shift between the model predictions and the observed colours for a sample of old Milky Way globular clusters reported by Cohen et al. (2007) is not observed in our Magellanic Cloud cluster analysis. The largest spread in colour is found for clusters in the age range $2 - 4$ Gyr. We believe that much of the spread in the colours for *individual*
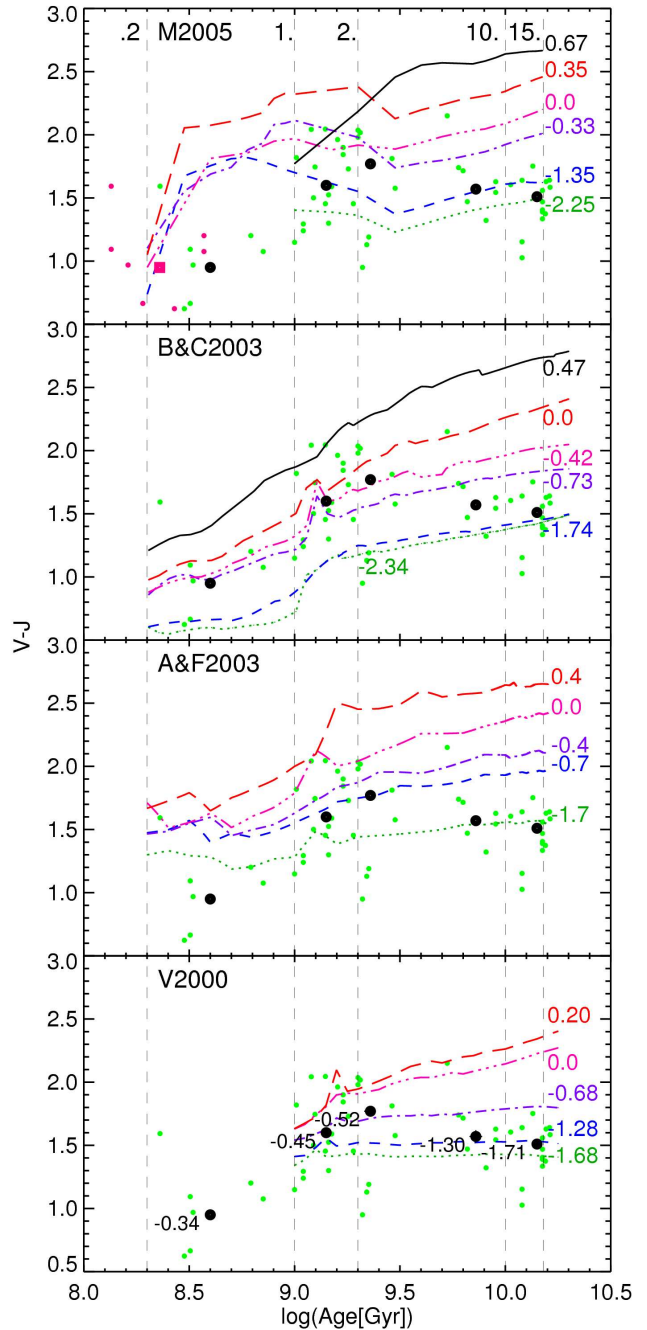
clusters younger than 10 Gyr results from stochastic fluctuations in the numbers of infrared-luminous stars, since individual clusters tend to have less than $\mathcal{M}_{(10\%)}$[6] contributing to the observed colours.

Composite $(B - J)_0$, $(V - J)_0$, and $(J - K_s)_0$ cluster colours are calculated for each age/metallicity interval, and compared with the predictions of four widely used population synthesis models (Maraston 2005; Bruzual & Charlot

---

[6] stellar mass needed to decrease the the luminosity uncertainty due to stochastic effects in the stellar population to 10%)

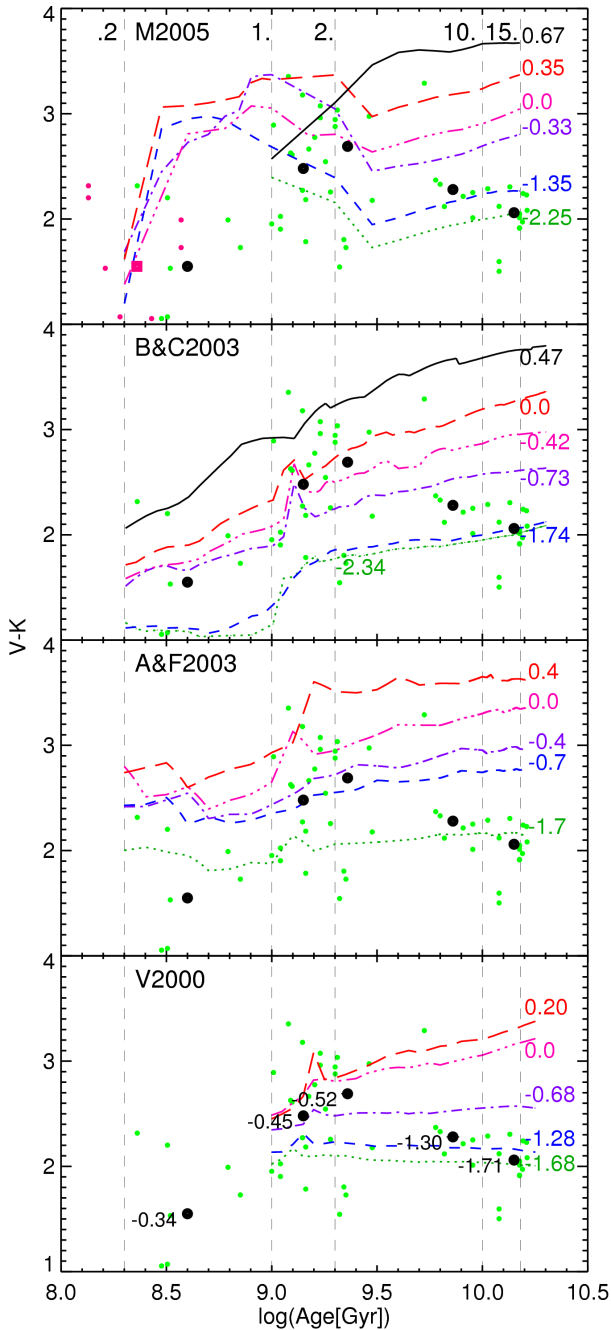**Figure 15.** The same as Figure 12, but for $(V - K_s)$ colour.

Figure 16. The same as Figure 12, but for $(J - K_s)$ colour.

2003; Anders & Fritze-v. Alvensleben 2003; Vazdekis 1999), in order to evaluate their performance. We interpolate the model grids to calculate the offset or distance in colour-colour space between the model predictions and the age and metallicity for our composite cluster colours. All four sets of models reproduce the colours of old ($\geqslant 10$ Gyr) Magellanic Cloud clusters quite well, with the Maraston (2005) and Bruzual & Charlot (2003) models giving slightly better fits than the other two.

In the age range of $2 - 10$ Gyr, the Maraston (2005) models have the largest separation in optical-NIR colour-colour space between the 2 Gyr and 10 Gyr model tracks,
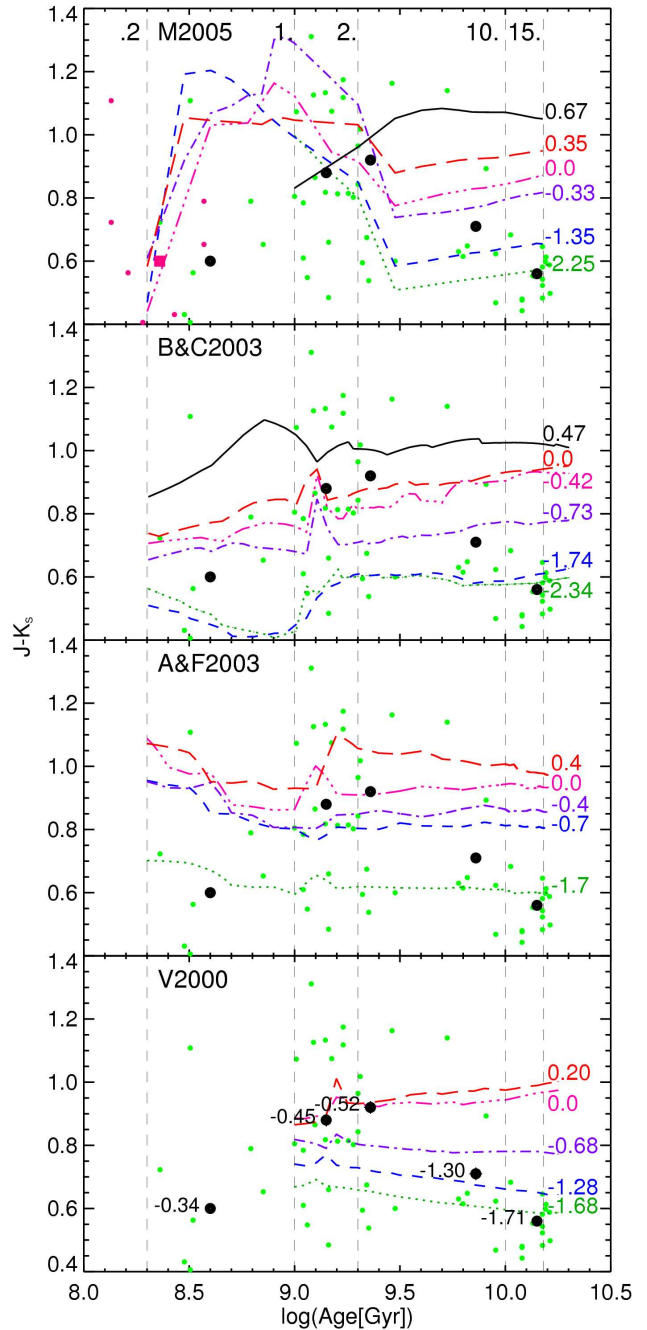
which best reproduces our observed composite colours in the $2 - 3$ Gyr and $3 - 9$ Gyr ranges. While the composite colour for $2 - 3$ Gyr-old clusters falls just off the grid for the other three models, actual quantitative distances between the model predictions and composite cluster colours are not significantly different among the four models. In the $1 - 2$ Gyr and $0.2 - 1$ Gyr age ranges, the Bruzual & Charlot (2003) models generally give the best quantitative match to our composite Magellanic Cloud cluster colours. Taking into account the inferred ages and metallicities, there is little difference between the Bruzual & Charlot (2003) and Maraston (2005) model performance. The cluster colours fall off the

Anders & Fritze-v. Alvensleben (2003) and Vazdekis (1999) model predictions in the two youngest age ranges, largely due to their limited coverage at low metallicities.

Based on the comparisons presented in this work, it is found that each model has strong and weak points when used to analyse the optical+NIR colours of unresolved stellar populations. There is no model set that clearly outperforms the others in all respects. Overall, the Bruzual & Charlot (2003) and typically yield the best quantitative match to our composite cluster colors. The Maraston (2005) models are a close second. The same two models also yield the best match to the composite cluster ages and metallicities.

ACKNOWLEDGMENTS

REFERENCES

Alcaino, G. 1978, A&AS, 34, 431

Alcaíno, G., Liller, W., Alvarado, F., Kravtsov, V., Ipatov, A., Samus, N., & Smirnov, O. 1999, A&AS, 135, 103

Alcaino, G., Alvarado, F., & Kurtev, R. 2003, A&A, 407, 919

Alves, D. R. 2004, New Astronomy Review, 48, 659

Alves, D. R., & Sarajedini, A. 1999, ApJ, 511, 225

Anders, P., & Fritze-v. Alvensleben, U. 2003, A&A, 401, 1063

Bernard, A. 1975, A&A, 40, 199

Bernard, A., & Bigay, J. H. 1974, A&A, 33, 123

Bertelli, G., Bressan, A., Chiosi, C., Fagotto, F., & Nasi, E. 1994, A&AS, 106, 275

Bessell, M. S., & Brett, J. M. 1988, PASP, 100, 1134

Bica, E., Dottori, H., & Pastoriza, M. 1986, A&A, 156, 261

Bica, E., Claria, J. J., Dottori, H., Santos, J. F. C., Jr., & Piatti, A. E. 1996, ApJS, 102, 57

Brocato, E., Castellani, V., Ferraro, F. R., Piersimoni, A. M., & Testa, V. 1996, MNRAS, 282, 614

Brown, T. M., Ferguson, H. C., Smith, E., Kimble, R. A., Sweigart, A. V., Renzini, A., Rich, R. M., & VandenBerg, D. A. 2004, ApJ, 613, L125

Bruzual A., G. 2002, IAU Symposium, 207, 616

Bruzual A, G. 2007, ArXiv Astrophysics e-prints, arXiv:astro-ph/0703052

Bruzual, A. G., & Charlot, S. 1993, ApJ, 405, 538

Bruzual, G., & Charlot, S. 2003, MNRAS, 344, 1000

Buzzoni, A. 1989, ApJS, 71, 817

Burstein, D., & Heiles, C. 1982, AJ, 87, 1165

Cardelli, J. A., Clayton, G. C., & Mathis, J. S. 1989, ApJ, 345, 245

Carpenter, J. M. 2001, AJ, 121, 2851

Carretta, E., Cohen, J. G., Gratton, R. G., & Behr, B. B. 2001, AJ, 122, 1469

Cerviño, M., & Luridiana, V. 2004, A&A, 413, 145

Chabrier, G. 2003, PASP, 115, 763

Chiosi, E., Vallenari, A., Held, E. V., Rizzi, L., & Moretti, A. 2006, A&A, 452, 179

Chiosi, E., & Vallenari, A. 2007, ArXiv Astrophysics e-prints, arXiv:astro-ph/0702281

Cohen, J. G., Hsieh, S., Metchev, S., Djorgovski, S. G., & Malkan, M. 2007, AJ, 133, 99

Crowl, H. H., Sarajedini, A., Piatti, A. E., Geisler, D., Bica, E., Clariá, J. J., & Santos, J. F. C., Jr. 2001, AJ, 122, 220

Da Costa, G. S., & Hatzidimitriou, D. 1998, AJ, 115, 1934

Dirsch, B., Richtler, T., Gieren, W. P., & Hilker, M. 2000, A&A, 360, 133

Elson, R. A. W., & Fall, S. M. 1985, ApJ, 299, 211

Elson, R. A., & Fall, S. M. 1988, AJ, 96, 1383

Ferraro, F. R., Montegriffo, P., Origlia, L., & Fusi Pecci, F. 2000, AJ, 119, 1282

Ferraro, F. R., Origlia, L., Testa, V., & Maraston, C. 2004, ApJ, 608, 772

Ferraro, F. R., Mucciarelli, A., Carretta, E., & Origlia, L. 2006, ApJL, 645, L33

Frogel, J. A., Persson, S. E., Matthews, K., & Aaronson, M. 1978, ApJ, 220, 75

Geisler, D., Bica, E., Dottori, H., Claria, J. J., Piatti, A. E., & Santos, J. F. C., Jr. 1997, AJ, 114, 1920

Girardi, L., Chiosi, C., Bertelli, G., & Bressan, A. 1995, A&A, 298, 87

Girardi, L., Bertelli, G., Bressan, A., Chiosi, C., Groenewegen, M. A. T., Marigo, P., Salasnich, B., & Weiss, A. 2002, A&A , 391, 195

Glass, I. S. 1985, Irish Astronomical Journal, 17, 1

Goudfrooij, P., Alonso, M. V., Maraston, C., & Minniti, D. 2001, MNRAS, 328, 237

Goudfrooij, P., Gilmore, D., Kissler-Patig, M., & Maraston, C. 2006, MNRAS, 369, 697

Grocholski, A., Alonso, A., Sarajedini, A., Geisler,D., & Smith, V. 2006, astro-ph/0607052

Harries, T. J., Hilditch, R. W., & Howarth, I. D. 2003, MNRAS, 339, 157

Harris, W. E. 1996, AJ, 112, 1487

Hempel, M., & Kissler-Patig, M. 2004, A&A, 419, 863

Hill, V., François, P., Spite, M., Primas, F., & Spite, F. 2000, A&A, 364, L19

Hunter, D. A., Elmegreen, B. G., Dupuy, T. J., & Mortonson, M. 2003, AJ, 126, 1836

Johnson, H. L. 1965, Communications of the Lunar and Planetary Laboratory, 3, 73

Johnson, H. L. 1966, ARA&A, 4, 193

Johnson, H. L., MacArthur, J. W., & Mitchell, R. I. 1968, ApJ, 152, 465

Johnson, J. A., Bolte, M., Stetson, P. B., Hesser, J. E., & Somerville, R. S. 1999, ApJ, 527, 199

Kerber, L. O., Santiago, B. X., & Brocato, E. 2007, A&A, 462, 139

Kroupa, P. 2001, MNRAS, 322, 231

Lançon, A., & Mouhcine, M. 2000, Massive Stellar Clusters,

211, 34

Mackey, A. D., & Gilmore, G. F. 2004, MNRAS, 352, 153

Mackey, A. D., Payne, M. J., & Gilmore, G. F. 2006, MN-RAS, 369, 921

Maraston, C. 1998, MNRAS, 300, 872

Maraston, C. 2005, MNRAS, 362, 799

McLaughlin, D. E., & van der Marel, R. P. 2005, ApJS, 161, 304

Mighell, K. J., Rich, R. M., Shara, M., & Fall, S. M. 1996, AJ, 111, 2314

Mighell, K. J., Sarajedini, A., & French, R. S. 1998, ApJL, 494, L189

Mighell, K. J., Sarajedini, A., & French, R. S. 1998, AJ, 116, 2395

Mould, J. R., Xystus, D. A., & Da Costa, G. S. 1993, ApJ, 408, 108

Mucciarelli, A., Ferraro, F. R., Origlia, L., & Fusi Pecci, F. 2007, ArXiv Astrophysics e-prints, arXiv:astro-ph/0701649

Nantais, J. B., Huchra, J. P., Barmby, P., Olsen, K. A. G., & Jarrett, T. H. 2006, AJ, 131, 1416

Olsen, K. A. G., Hodge, P. W., Mateo, M., Olszewski, E. W., Schommer, R. A., Suntzeff, N. B., & Walker, A. R. 1998, MNRAS, 300, 665

Olszewski, E. W., Schommer, R. A., Suntzeff, N. B., & Harris, H. C. 1991, AJ, 101, 515

Olszewski, E. W., Suntzeff, N. B., & Mateo, M. 1996, ARA&A, 34, 511

Persson, S. E., Aaronson, M., Cohen, J. G., Frogel, J. A., & Matthews, K. 1983, ApJ, 266, 105

Pessev, P. M., Goudfrooij, P., Puzia, T. H., & Chandar, R. 2006, AJ, 132, 781

Puzia, T. H., Zepf, S. E., Kissler-Patig, M., Hilker, M., Minniti, D., & Goudfrooij, P. 2002, A&A, 391, 453

Puzia, T. H., Mobasher, B., & Goudfrooij, P. 2007, ArXiv e-prints, 705, arXiv:0705.4092

Rich, R. M., Shara, M. M., & Zurek, D. 2001, AJ, 122, 842

Salpeter, E. E. 1955, ApJ, 121, 161

Sarajedini, A. 1994, AJ, 107, 618

Skrutskie, M. F., et al. 2006, AJ, 131, 1163

Spergel, D. N., et al. 2006, arXiv:astro-ph/0603449

Testa, V., Ferraro, F. R., Brocato, E., & Castellani, V. 1995, MNRAS, 275, 454

Vandenberg, D. A. 1985, ApJS, 58, 711

Vandenberg, D. A., Bolte, M., & Stetson, P. B. 1990, AJ, 100, 445

van den Bergh, S. 1981, A&AS, 46, 79

van den Bergh, S., & Hagen, G. L. 1968, AJ, 73, 569

van der Wel, A., Franx, M., van Dokkum, P. G., Huang, J., Rix, H.-W., & Illingworth, G. D. 2006, ApJ, 636, L21

Vallenari, A., Aparicio, A., Fagotto, F., & Chiosi, C. 1994, A&A, 284, 424

Vazdekis, A. 1999, ApJ, 513, 224

Walker, A. R. 1992, AJ, 104, 1395

Whitmore, B. C., Chandar, R., & Fall, S. M. 2007, AJ, 133, 1067

Wolf, M. J., Drory, N., Gebhardt, K., & Hill, G. J. 2007, ApJ, 655, 179

Woo, J.-H., Gallart, C., Demarque, P., Yi, S., & Zoccali, M. 2003, AJ, 125, 754

Worthey, G. 1994, ApJS, 95, 107

Zaritsky, D., Harris, J., & Thompson, I. 1997, AJ, 114, 1002

Table A7. Ages and S parameter values for the clusters from the Kerber et al. 2007 sample ($25 \leqslant S \leqslant 40$).

Cluster ID (1)	S (2)	Girardi et al. 1995 $\log(\tau)$ (3)	Kerber et al. 2007 $\log(\tau)$ (4)	This paper $\log(\tau)$ (5)
NGC1651	38	9.00 ± 0.14	9.30 ± 0.03	9.23 ± 0.12
NGC1718	40	9.15 ± 0.14	9.31 ± 0.03	9.38 ± 0.12
NGC1777	38	9.00 ± 0.14	9.06 ± 0.04	9.23 ± 0.12
NGC1831	32	8.56 ± 0.14	8.85 ± 0.05	8.79 ± 0.12
NGC1856	30	8.42 ± 0.14	8.47 ± 0.04	8.65 ± 0.12
NGC1868	33	8.64 ± 0.14	9.05 ± 0.03	8.87 ± 0.12
NGC2162	37	8.93 ± 0.14	9.10 ± 0.03	9.16 ± 0.12
NGC2209	34	8.71 ± 0.14	9.08 ± 0.03	8.94 ± 0.12
NGC2213	38	9.00 ± 0.14	9.23 ± 0.04	9.23 ± 0.12
NGC2249	33	8.64 ± 0.14	9.00 ± 0.03	8.87 ± 0.12
SL506	40	9.15 ± 0.14	9.35 ± 0.03	9.38 ± 0.12
NGC265	26	8.13 ± 0.14	8.5 ± 0.3	8.36 ± 0.12

Notes to Table A7: Column (1) is the cluster ID. The S parameter value and the corresponding age according to Girardi et al. (1995) are listed in columns (2) and (3). Column (4) is the $\log(\tau)$ for the clusters from Kerber et al. (2007). The age derived by our calibration are given in column (5).

Zaritsky, D., Harris, J., Thompson, I. B., Grebel, E. K., & Massey, P. 2002, AJ, 123, 855

Zaritsky, D., Harris, J., Thompson, I. B., & Grebel, E. K. 2004, AJ, 128, 1606

APPENDIX A: S PARAMETER - AGE RE-CALIBRATION

There are currently very few CMD based ages for Magellanic Cloud clusters in our youngest age bin (200 Myr-1 Gyr). One possible solution is to use the "S-parameter" calibration for LMC clusters, which would allow us to select additional clusters for analysis in §3.4. The S-parameter, introduced by Elson & Fall (1985), provides an empirical relation between the age of a cluster and its integrated $(U - B)$ vs. $(B - V)$ colours. Girardi et al. (1995) revised the S-parameter-age calibration based on 24 clusters which had age estimates from high quality *(at the time)* ground-based CCD observations. They obtained the following relation between S and cluster age (in $\log(\tau)$):

$$log(\tau/[years]) = (0.0733 \pm 0.0032) * S + 6.227 \pm 0.096 \quad (A1)$$

With a rms dispersion in $\log(\tau)$ equal to 0.137.

We performed an independent analysis of the S-parameter using new age estimates for Magellanic Cloud clusters derived from HST-based CMDs by Kerber et al. (2007). These include the age range for which we have few CMD-based ages (~ 0.3 Gyr to ~ 1 Gyr). The optical colours from Table 4 were used to derive S parameter values according to the definition given by Girardi et al. (1995). A comparison between the Kerber et al. and Girardi et al. age estimates for 12 clusters shows that there is an offset, such that the Kerber et al. ages are systematically older. The uncertainty weighted mean offset of the Kerber et al. ages from the Girardi et al. calibration is 0.235 in $\log(\tau)$. We confirmed that the difference between the age estimates is *not* caused
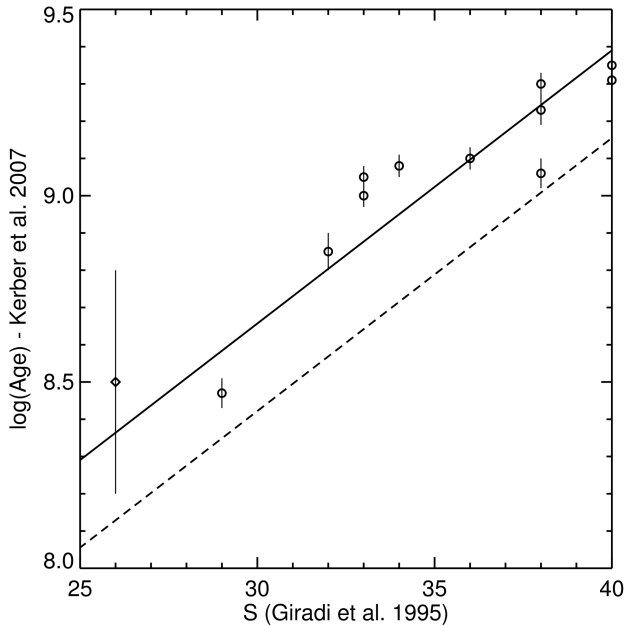
Figure A17. Ages from Kerber et al. 2007 and Chiosi & Vallenari 2007 as function of the S parameter. The dashed line represent Girardi et al. 1995 calibration. NGC265 (indicated with a diamond) was added to improve the sampling in the 200 Myr - 1 Gyr age interval. The weighted mean offset of the data points with respect of the original relation is shown with a solid line.

Table A8. Extention of the sample based on the S parameter.

ID (1)	S (2)	$\log(\tau)$ (3)	ID (1)	S (2)	$\log(\tau)$ (3)
NGC1866	27	8.43 ± 0.12	NGC1644	37	9.16 ± 0.12
NGC2031	26	8.36 ± 0.12	NGC1783	37	9.16 ± 0.12
NGC2107	32	8.79 ± 0.12	NGC1987	35	9.01 ± 0.12
NGC2134	28	8.50 ± 0.12	NGC2108	36	9.09 ± 0.12
NGC2156	28	8.50 ± 0.12	NGC2154	38	9.23 ± 0.12

Notes to Table A8: Column (1) is the cluster ID. Column (2) lists the derived S parameter values, along with the calculated ages in column (3).

by the adoption of different stellar isochrones (Bertelli et al. 1994; Girardi et al. 2002, respectively for studies of Girardi et al. and Kerber et al.), since they are indistinguishable from each other in the B and V bands which were used by Kerber et al. (2007). Kerber et al. have better data and apply a more robust technique for age determination, therefore we recalibrate the cluster ages with the appropriate offset:

$$log(\tau/[years]) = 0.0733 * S + 6.458 \qquad (A2)$$

The standard deviation of Kerber et al. (2007) data around the new relation is $\sigma = 0.123$.

The objects selected to extend the sample based on the S parameter values from equation A2 are listed in Table A8.

APPENDIX B: DEFINING THE TEST SAMPLE

In order to test the performance of SSP models we need to define a reliable test sample: Objects with age and metallicity measurements based on high-quality data, covering an appropriate parameter space. We prefer age and metallicity estimates based on CMDs, particularly those taken with *HST*, but also include metallicity estimates from individual stars, integrated spectroscopy and age estimates for the youngest two age bins from the S-parameter (described in Appendix A). In order to clarify possible age-related effects in the SSP models performance, we decided to split the sample into several age bins: *(i)* Globular clusters older than 10 Gyr; *(ii)* Clusters with ages between 2 and 10 Gyr; *(iii)* Clusters older than 1 Gyr and younger than 2 Gyr; *(iv)* Clusters with ages between 200 Myr and 1 Gyr. The latter two age bins are where the effects of AGB and RGB stars on the NIR integrated-light properties are most pronounced.

The intrinsic spread in integrated colours for clusters with a given age and metallicity increases with decreasing mass (Bruzual A. (2002), due to stochastic fluctuations in the number of massive stars. Therefore, we consider clusters with masses exceeding $\mathcal{M}_{(10\%)}$ to be reliable test particles. Since many clusters (particularly in the youngest age bins) have mass estimates lower than this value, we also present cumulative colours for each age bin, where the measured colours correspond to masses exceeding this limit.

B1 The Old Cluster Population (Ages $\geqslant$ 10 Gyr)

Olszewski et al. (1996) listed 14 LMC clusters believed to be as old as the oldest Galactic globulars. More recent studies have established that ESO 121-SC03 should be excluded from their original list, since it is somewhat younger at 8.3-9.8 Gyr (Mackey et al. 2006), (given that the typical age of a Galactic globular cluster exceeds 10 Gyr). On the other hand the two "suspected" old globulars, NGC 1928 and NGC 1939, were confirmed (see references below), giving a total of 15 ancient globular clusters in the LMC. NGC 121 is the only known old globular cluster in the SMC (Mighell et al. 1998b). The adopted age and metallicity for each cluster, with associated references, are listed in Table B9. The table is supplemented with extinction information based on individual cluster CMDs and values retrieved from MCPS Zaritsky et al. ((1997). The estimated stellar mass which contributes to the integrated-light measurements for each cluster (based on our 2MASS J band integrated-light photometry and mass-to-light ratios from Maraston (2005)) are listed in Column 7 of Table B10, and are lower than the total cluster masses. Total cluster mass estimates from McLaughlin & van der Marel (2005) are also given.

We believe that the following ten old clusters are reliable test particles: 4 inner LMC objects (NGC1786, NGC1835, NGC1898, NGC2019); one outer LMC cluster (NGC2210), and NGC121 in the SMC. The other three outer objects (NGC1841, NGC2257, Hodge11) have integrated light measurements taken in apertures (set by the optical dataset) which sample only a fraction of the total stellar population in each cluster. The stellar mass which contributes to the integrated light measurements are lower than $\mathcal{M}_{(10\%)}$, and therefore these clusters may have a larger spread in colour-colour space.

Table B9. Information about the cluster test sample.

Cluster ID (1)	[Fe/H] (2)		Age (3)		$E(B-V)$ (4)		$E(V-I)$ (5)		$A_{V(\text{CMD})}$ (6)	$A_{V(\text{MCPS})}$ (7)	Note (8)
Old globular clusters (Ages $\geqslant$ 10 Gyr)											
LMC											
NGC1466	-1.85 ± 0.1	(22)	$15 \ \pm 3$	(11)	$0.09 \ \pm 0.02$	(22)			0.28 ± 0.06	0.39 ± 0.02	O
NGC1754	-1.42 ± 0.15	(18)	15.6 ± 2.2	(18)	$0.09 \ \pm 0.02$	(18)			0.28 ± 0.06	0.40 ± 0.04	I
NGC1786	$-2.1 \ \pm 0.3$	(2)	$15 \ \pm 3$	(2)	$0.09 \ \pm 0.05$	(2)	0.12 ± 0.05	(2)	0.28 ± 0.16	0.62 ± 0.04	I
NGC1835	-1.62 ± 0.15	(18)	16.2 ± 2.8	(18)	$0.08 \ \pm 0.02$	(18)			0.25 ± 0.06	0.35 ± 0.07	I
NGC1841	$-2.2 \ \pm 0.2$	(2)	$15 \ \pm 3$	(2)	0.20 ± 0.03	(2)	0.28 ± 0.03	(2)	0.62 ± 0.09	0.39 ± 0.02	O
NGC1898	-1.18 ± 0.16	(18)	13.5 ± 2.2	(18)	$0.07 \ \pm 0.02$	(18)			0.22 ± 0.06	0.43 ± 0.05	I
NGC1916										0.42 ± 0.05	I
NGC1928	-1.27 ± 0.14	(13)	$GC \pm 2$	(13)			0.08 ± 0.02	(13)	0.20 ± 0.05	0.43 ± 0.03	I
NGC1939	-2.10 ± 0.19	(13)	$GC \pm 2$	(13)			0.16 ± 0.03	(13)	0.40 ± 0.08	0.62 ± 0.05	I
NGC2005	-1.35 ± 0.16	(18)	15.5 ± 4.9	(18)	$0.12 \ \pm 0.02$	(18)			0.37 ± 0.06	0.47 ± 0.04	I
NGC2019	-1.23 ± 0.15	(18)	16.3 ± 3.1	(18)	$0.12 \ \pm 0.02$	(18)			0.37 ± 0.06	0.44 ± 0.06	I
NGC2210	$-2.2 \ \pm 0.2$	(2)	$15 \ \pm 3$	(2)	$0.09 \ \pm 0.03$	(2)	0.12 ± 0.03	(2)	0.28 ± 0.09	0.39 ± 0.02	O
NGC2257	$-1.7 \ \pm 0.2$	(21)	$10 - 14$	(21)	0.0	(21)			0.00 ± 0.00	0.39 ± 0.02	O
Hodge11	-2.06 ± 0.2	(15)	$15 \ \pm 3$	(15)	0.075 ± 0.005	(15)			0.23 ± 0.02	0.39 ± 0.02	O
Reticulum	-1.66 ± 0.12	(13)	$GC \pm 2$	(13)			0.07 ± 0.02	(13)	0.18 ± 0.05	0.39 ± 0.02	O
SMC											
NGC121	-1.71 ± 0.10	(16)	10.6 ± 0.7	(16)	$0.05 \ \pm 0.03$	(16)			0.16 ± 0.09	0.18 ± 0.01	
Cluster with 2 Gyr $\leqslant$ Ages < 10 Gyr											
LMC											
NGC1651	-0.53 ± 0.03	(9)	2.00 ± 0.15	(12)	0.11 ± 0.01	(12)			0.34 ± 0.03	0.35 ± 0.05	
NGC1718	-0.80 ± 0.03	(9)	2.05 ± 0.15	(12)	0.10 ± 0.03	(12)			0.31 ± 0.09	0.51 ± 0.06	
NGC2121	-0.50 ± 0.03	(9)	2.90 ± 0.50	(12)	0.07 ± 0.02	(12)			0.22 ± 0.06	0.53 ± 0.04	
NGC2155	-0.50 ± 0.05	(9)	3.00 ± 0.25	(12)	0.02 ± 0.01	(12)			0.06 ± 0.03	0.43 ± 0.04	
NGC2193	-0.49 ± 0.05	(9)	$2.2 \ \pm 0.5$	(20)						0.39 ± 0.02	
SL663	-0.54 ± 0.05	(9)	3.15 ± 0.40	(12)	0.07 ± 0.02	(12)			0.22 ± 0.06	0.38 ± 0.04	
SL842	-0.36 ± 0.20	(19)	2.0	(8)						0.39 ± 0.02	
Hodge4	-0.55 ± 0.06	(9)	$2.1 \ \pm 0.3$	(23)						0.39 ± 0.02	
Hodge14	-0.45 ± 0.10	(12)	2.25 ± 0.15	(12)	0.08 ± 0.02	(12)			0.25 ± 0.06	0.39 ± 0.02	
ESO121-03	-0.97 ± 0.10	(12)	$8.3 - 9.8$	(12)			0.04 ± 0.02	(13)	0.10 ± 0.05	0.39 ± 0.02	
SMC											
NGC339	-1.50 ± 0.14	(16)	6.3 ± 1.3	(16)	0.03 ± 0.04	(16)			0.09 ± 0.12	0.18 ± 0.01	
NGC361	-1.45 ± 0.11	(16)	8.1 ± 1.2	(16)	0.07 ± 0.03	(16)			0.22 ± 0.09	0.17 ± 0.02	
NGC416	-1.44 ± 0.12	(15)	6.6 ± 0.5	(15)	0.08 ± 0.03	(15)			0.25 ± 0.09	0.20 ± 0.02	
Kron3	-1.12 ± 0.12	(6)	6.0 ± 1.3	(16)	$-0.03 \pm 0.02^*$	(16)			0.00 ± 0.06	0.18 ± 0.01	
Lindsay1	-1.17 ± 0.10	(6)	9.0 ± 1.0	(16)	0.06 ± 0.02	(16)			0.19 ± 0.06	0.18 ± 0.01	
Lindsay113	-1.44 ± 0.16	(6)	5.3 ± 1.3	(16)	0.00 ± 0.02	(16)			0.00 ± 0.06	0.18 ± 0.01	
Cluster with 1 Gyr $\leqslant$ Ages < 2 Gyr											
LMC											
NGC1644	-0.3	(*)	$1.45^{+0.46}_{-0.35}$	(*)						0.39 ± 0.02	
NGC1777	-0.60 ± 0.10	(12)	1.15 ± 0.15	(12)	0.10 ± 0.03	(12)			0.31 ± 0.09	0.39 ± 0.02	
NGC1783	-0.3	(*)	$1.45^{+0.46}_{-0.35}$	(*)						0.30 ± 0.03	
NGC1868	-0.70 ± 0.10	(12)	1.10 ± 0.10	(12)	0.04 ± 0.01	(12)			0.12 ± 0.03	0.39 ± 0.02	
NGC1978	-0.38 ± 0.07	(7)	$1.9 \ \pm 0.1$	(17)						0.76 ± 0.05	
NGC1987	-0.3	(*)	$1.02^{+0.33}_{-0.23}$	(*)						0.28 ± 0.03	
NGC2108	-0.3	(*)	$1.23^{+0.39}_{-0.30}$	(*)						0.50 ± 0.05	
NGC2154	-0.4	(*)	$1.70^{+0.54}_{-0.41}$	(*)						0.39 ± 0.03	
NGC2162	-0.46 ± 0.07	(9)	1.25 ± 0.10	(12)	0.03 ± 0.02	(12)			0.09 ± 0.06	0.39 ± 0.02	
NGC2173	-0.42 ± 0.03	(9)	1.60 ± 0.20	(12)	0.07 ± 0.02	(12)			0.22 ± 0.06	0.39 ± 0.02	

Notes to Table B9: See next page.

Table B9. Continued

Cluster ID (1)	[Fe/H] (2)		Age (3)		$E(B-V)$ (4)		$E(V-I)$ (5)		$A_{V(\rm CMD)}$ (6)	$A_{V(\rm MCPS)}$ (7)	Note (8)
Cluster with 1 Gyr $\leqslant$ Ages $<$ 2 Gyr											
LMC											
NGC2190	-0.12 ± 0.20	(19)	1.1	(8)						0.39 ± 0.02	
NGC2203	-0.41 ± 0.03	(9)	1.8	(8)						0.39 ± 0.02	
NGC2209	-0.50 ± 0.10	(12)	1.20 ± 0.10	(12)	0.15 ± 0.03	(12)			0.47 ± 0.09	0.39 ± 0.02	
NGC2213	-0.52 ± 0.04	(9)	1.70 ± 0.20	(12)	0.06 ± 0.03	(12)			0.19 ± 0.09	0.40 ± 0.04	
NGC2231	-0.52 ± 0.04	(9)	1.5	(8)						0.39 ± 0.02	
NGC2249	-0.45 ± 0.10	(12)	1.00 ± 0.10	(12)	0.01 ± 0.02	(12)			0.03 ± 0.06	0.39 ± 0.02	
SMC											
NGC152	-0.94 ± 0.15	(4)	1.4 ± 0.2	(4)	0.05 ± 0.01	(4)			0.16 ± 0.03	0.19 ± 0.02	
NGC411	-0.68 ± 0.07	(1)	1.4 ± 0.2	(1)	0.12 ± 0.01	(4)			0.37 ± 0.03	0.17 ± 0.02	
Cluster with 0.2 Gyr $\leqslant$ Ages $<$ 1 Gyr											
LMC											
NGC1831	-0.10 ± 0.10	(12)	$0.71^{+0.09}_{-0.08}$	(12)	0.11 ± 0.01	(12)			0.34 ± 0.03	0.39 ± 0.02	
NGC1856	-0.40 ± 0.10	(12)	0.30 ± 0.03	(12)	0.21 ± 0.02	(12)			0.65 ± 0.06	0.22 ± 0.03	
NGC1866	-0.50 ± 0.10	(10)	$0.33^{+0.09}_{-0.07}$	(*)						0.28 ± 0.06	
NGC2031	-0.52 ± 0.21	(5)	$0.23^{+0.07}_{-0.06}$	(*)						0.40 ± 0.03	
NGC2107	-0.2	(*)	$0.62^{+0.19}_{-0.15}$	(*)						0.36 ± 0.04	
NGC2134	-0.2	(*)	$0.32^{+0.10}_{-0.08}$	(*)						0.62 ± 0.03	
NGC2156	-0.2	(*)	$0.32^{+0.10}_{-0.08}$	(*)						0.20 ± 0.02	
SMC											
NGC265	$-0.62^{+0.23}_{-0.61}$	(3)	$0.32^{+0.32}_{-0.16}$	(3)			$0.06^{+0.05}_{-0.04}$	(3)	$0.19^{+0.15}_{-0.13}$	0.34 ± 0.02	

Notes to Table B9: Column (1) - cluster designation. Columns (2) and (3) are the metallicity and the age of the cluster with corresponding references given in parenthesis. Reddening information based on CMDs plus corresponding references is listed in columns (4), (5) and (6). A_V retrieved from MCPS database is presented in column (7). Finally, notes are given in column (8)

In column (8) I and O stands for the positions of the objects in the LMC. I means inner (bar) and O outer clusters. There are slight variations in this classification from author to author. Here we classify the objects as in Mackey & Gilmore (2004).

Mackey & Gilmore (2004) concluded that NGC1928, NGC1939 and Reticulum are coeval in age with the oldest Milky Way globular clusters within 2 Gyr. In the table this result is denoted as "$GC \pm 2$".

ESO121-SC03 is the only object in the LMC age-metallicity gap. It is younger than the genuine old globular clusters, but significantly older than the intermediate-age massive clusters from this galaxy. It'll be compared with the model predictions alongside with the objects from the next age bin.

References: (1)Alves & Sarajedini (1999) (2)Brocato et al. (1996) (3)Chiosi & Vallenari (2007) (4)Crowl et al. (2001) (5)Dirsch et al. (2000) (6)Da Costa & Hatzidimitriou (1998) (7)Ferraro et al. (2006) (8)Geisler et al. (1997) (9)Grocholski et al. (2006) (10)Hill et al. (2000) (11)Johnson et al. (1999) (12)Kerber et al. (2007) (13)Mackey & Gilmore (2004) (14)Mackey et al. (2006) (15)Mighell et al. (1996) (16)Mighell et al. (1998b) (17)Mucciarelli et al. (2007) (18)Olsen et al. (1998) (19)Olszewski et al. (1991) (20)Rich et al. (2001) (21)Testa et al. (1995) (22)Walker (1992) (23)Woo et al. (2003)

Here, we provide more details on the available cluster age and metallicity information. Olsen et al. (1998) studied NGC 1754, 1835, 1898, 1916, 2005 and 2019. Their F555W and F814W WFPC2 CMDs reach an apparent magnitude $V \approx 25$, well below the MSTO point. The metallicities were derived using the technique of (Sarajedini 1994, ; hereafter S94). In most cases there is good agreement between the photometric results of Olsen et al. (1998) and the spectroscopy of individual cluster members of Olszewski et al. (1991). For the clusters showing large discrepancies (NGC 2005 and NGC 2019) the metallicities in Olszewski et al. are significantly lower, although Olszewski et al. do note that the measurements for these clusters are uncertain. Grocholski et al. (2006) recently estimated [Fe/H] $= -1.31 \pm 0.05$ for

NGC 2019 based on moderate resolution Ca II Triplet spectroscopy of 5 cluster stars, in good agreement with the result of Olsen et al. ([Fe/H]$=-1.23 \pm 0.15$). Age estimates relative to those of MW GCs with similar metallicity were measured according to the method of Vandenberg et al. (1990).

Another three old LMC clusters (NGC1466, NGC2257, and Hodge11) were observed with WFPC2 F555W and F814W filters by Johnson et al. (1999). In this case the authors did not attempt to derive their own metallicity estimates, but adopted already published values instead.

Mackey & Gilmore (2004) published ACS Wide Field Channel (WFC) F555W and F814W photometry for NGC 1928, 1939 (clusters located in the LMC bar region), and for the remote outer cluster Reticulum. Employing the S94

Table B10. 2MASS integrated-light photometry and mass estimates.

Cluster ID (1)	D (2)	J (3)	H (4)	K_S (5)	$log(m)_{\rm NIR}$ (6)	$log(m)_{\rm Lit}$ (7)
Old globular clusters (Ages $\geqslant$ 10 Gyr)						
LMC						
NGC1466	60	9.83 ± 0.02	9.39 ± 0.01	9.30 ± 0.01	5.18 ± 0.07	5.24 ± 0.04
NGC1754	100	9.74 ± 0.06	9.24 ± 0.04	9.08 ± 0.05	$5.22^{+0.06}_{-0.08}$	5.07 ± 0.05
NGC1786	60	8.57 ± 0.01	8.09 ± 0.01	8.00 ± 0.01	$5.70^{+0.14}_{-0.22}$	5.57 ± 0.05
NGC1835	60	8.34 ± 0.01	7.82 ± 0.01	7.71 ± 0.01	5.77 ± 0.08	5.71 ± 0.05
NGC1841	25	12.23 ± 0.02	11.69 ± 0.02	11.48 ± 0.02	$4.28^{+0.05}_{-0.06}$	$5.31^{+0.07}_{-0.06}$
NGC1898	62	9.52 ± 0.02	9.18 ± 0.03	9.00 ± 0.03	$5.30^{+0.08}_{-0.09}$	5.35 ± 0.06
NGC1916	44	8.36 ± 0.01	7.91 ± 0.01	7.68 ± 0.01	$5.79^{+0.04}_{-0.05}$	5.77 ± 0.05
NGC1928	62	10.71 ± 0.09	10.27 ± 0.12	10.20 ± 0.15	$4.83^{+0.07}_{-0.09}$	
NGC1939	38	10.34 ± 0.02	9.89 ± 0.02	9.83 ± 0.02	$5.01^{+0.06}_{-0.07}$	
NGC2005	25	9.93 ± 0.01	9.39 ± 0.01	9.27 ± 0.01	5.15 ± 0.06	5.27 ± 0.05
NGC2019	60	9.10 ± 0.02	8.65 ± 0.02	8.54 ± 0.02	$5.49^{+0.05}_{-0.07}$	5.47 ± 0.05
NGC2210	62	9.25 ± 0.01	8.72 ± 0.01	8.66 ± 0.01	$5.43^{+0.09}_{-0.11}$	5.40 ± 0.05
NGC2257	61	10.98 ± 0.02	10.60 ± 0.03	10.50 ± 0.03	$4.71^{+0.03}_{-0.04}$	$5.00^{+0.12}_{-0.07}$
Hodge11	62	10.48 ± 0.02	9.88 ± 0.02	9.86 ± 0.02	4.93 ± 0.03	$5.17^{+0.07}_{-0.06}$
SMC						
NGC121	62	9.52 ± 0.01	8.90 ± 0.01	8.81 ± 0.01	$5.45^{+0.15}_{-0.21}$	5.57 ± 0.04
Cluster with 2 Gyr $\leqslant$ Ages $<$ 10 Gyr						
LMC						
NGC1651	100	10.00 ± 0.02	9.23 ± 0.02	9.10 ± 0.02	4.43 ± 0.04	$4.53^{+0.11}_{-0.09}$
NGC1718	62	10.01 ± 0.01	9.13 ± 0.01	8.94 ± 0.01	$4.44^{+0.08}_{-0.10}$	4.57 ± 0.22
NGC2121	62	10.40 ± 0.03	9.73 ± 0.03	9.20 ± 0.02	$4.50^{+0.08}_{-0.10}$	$5.00^{+0.08}_{-0.07}$
NGC2155	62	10.98 ± 0.02	10.31 ± 0.11	10.37 ± 0.03	$4.25^{+0.13}_{-0.18}$	$4.56^{+0.09}_{-0.08}$
NGC2193	38	12.01 ± 0.05	11.36 ± 0.04	11.27 ± 0.04	$3.64^{+0.03}_{-0.04}$	4.13 ± 0.08
SL663*	60	11.22 ± 0.02	11.08 ± 0.04	11.02 ± 0.04	$4.18^{+0.08}_{-0.10}$	$4.67^{+2.49}_{-0.45}$
SL842	38	11.89 ± 0.07	11.14 ± 0.05	10.86 ± 0.05	$3.67^{+0.03}_{-0.04}$	3.91 ± 0.10
Hodge4	38	12.10 ± 0.02	11.78 ± 0.06	11.44 ± 0.05	$3.60^{+0.03}_{-0.04}$	$5.31^{+1.91}_{-0.45}$
Hodge14	62	12.05 ± 0.03	11.37 ± 0.03	11.47 ± 0.04	$3.61^{+0.07}_{-0.08}$	4.00 ± 0.09
ESO121-03	61	12.34 ± 0.09	11.59 ± 0.07	11.70 ± 0.08	$4.02^{+0.14}_{-0.18}$	
SMC						
NGC339	62	11.06 ± 0.02	10.70 ± 0.02	10.43 ± 0.02	$4.57^{+0.28}_{-0.99}$	4.90 ± 0.07
NGC361	62	10.76 ± 0.02	9.97 ± 0.01	9.83 ± 0.02	$4.78^{+0.11}_{-0.15}$	$5.30^{+0.10}_{-0.08}$
NGC416	62	9.77 ± 0.01	9.16 ± 0.01	9.08 ± 0.01	$5.10^{+0.10}_{-0.13}$	5.21 ± 0.05
Kron3	62	10.31 ± 0.01	9.69 ± 0.01	9.68 ± 0.01	4.85 ± 0.03	5.15 ± 0.06
Lindsay1	62	11.64 ± 0.03	11.26 ± 0.03	11.14 ± 0.04	$4.45^{+0.09}_{-0.11}$	
Lindsay113	62	11.46 ± 0.02	10.49 ± 0.01	10.32 ± 0.01	4.35 ± 0.03	
Cluster with 1 Gyr $\leqslant$ Ages $<$ 2 Gyr						
LMC						
NGC1644	60	11.31 ± 0.11	10.88 ± 0.10	10.76 ± 0.10	$3.96^{+0.03}_{-0.04}$	
NGC1777	38	9.06 ± 0.01	8.59 ± 0.01	8.46 ± 0.01	$4.52^{+0.08}_{-0.10}$	4.28 ± 0.11
NGC1783	60	9.23 ± 0.01	8.62 ± 0.01	8.52 ± 0.01	$4.77^{+0.04}_{-0.05}$	
NGC1868	62	10.19 ± 0.01	9.71 ± 0.01	9.56 ± 0.01	$4.10^{+0.07}_{-0.09}$	4.33 ± 0.18
NGC1978	60	8.74 ± 0.02	8.04 ± 0.01	7.81 ± 0.02	4.97 ± 0.04	
NGC1987	60	10.16 ± 0.02	9.48 ± 0.01	9.04 ± 0.01	$4.21^{+0.04}_{-0.05}$	
NGC2108	62	10.46 ± 0.02	9.70 ± 0.02	9.25 ± 0.02	$4.22^{+0.04}_{-0.05}$	
NGC2154	62	10.14 ± 0.02	9.36 ± 0.01	8.90 ± 0.01	4.30 ± 0.04	
NGC2162	62	10.89 ± 0.04	10.21 ± 0.03	10.01 ± 0.03	$3.74^{+0.16}_{-0.26}$	4.02 ± 0.15
NGC2173	150	9.76 ± 0.10	9.10 ± 0.07	8.91 ± 0.07	$4.38^{+0.07}_{-0.09}$	4.70 ± 0.07

Notes to Table B10: See next page.

Table B10. 2MASS integrated-light photometry and mass estimates.

Cluster ID (1)	D (2)	J (3)	H (4)	K_S (5)	$log(m)_{\rm NIR}$ (6)	$log(m)_{\rm Lit}$ (7)
Cluster with 1 Gyr $\leqslant$ Ages $<$ 2 Gyr						
LMC						
NGC2190	61	11.42 ± 0.04	10.79 ± 0.04	10.57 ± 0.04	$3.64^{+0.03}_{-0.04}$	
NGC2203	150	9.28 ± 0.07	8.61 ± 0.05	8.40 ± 0.05	$4.42^{+0.03}_{-0.04}$	
NGC2209	62	10.77 ± 0.04	9.90 ± 0.04	9.38 ± 0.03	$3.84^{+0.06}_{-0.07}$	$4.36^{+2.59}_{-0.31}$
NGC2213	62	10.40 ± 0.02	9.55 ± 0.01	9.25 ± 0.01	$4.13^{+0.12}_{-0.17}$	4.30 ± 0.10
NGC2231	44	11.33 ± 0.08	10.51 ± 0.05	10.19 ± 0.04	$3.78^{+0.03}_{-0.04}$	4.36 ± 0.12
NGC2249	36	11.06 ± 0.05	10.57 ± 0.05	10.25 ± 0.04	$3.67^{+0.37}_{-....}$	4.03 ± 0.20
SMC						
NGC152	62	10.78 ± 0.02	9.95 ± 0.01	9.62 ± 0.01	$4.17^{+0.06}_{-0.07}$	4.56 ± 0.09
NGC411	62	10.49 ± 0.03	9.84 ± 0.03	9.61 ± 0.03	4.28 ± 0.04	4.47 ± 0.10
Cluster with 0.2 Gyr $\leqslant$ Ages $<$ 1 Gyr						
LMC						
NGC1831	60	9.86 ± 0.01	9.34 ± 0.01	9.15 ± 0.01	4.16 ± 0.04	4.59 ± 0.18
NGC1856	60	8.98 ± 0.02	8.59 ± 0.02	8.44 ± 0.02	4.26 ± 0.04	4.88 ± 0.12
NGC1866	60	8.72 ± 0.01	8.28 ± 0.01	8.11 ± 0.01	$4.34^{+0.07}_{-0.08}$	4.91 ± 0.12
NGC2031	72	8.95 ± 0.03	8.28 ± 0.03	8.16 ± 0.04	4.45 ± 0.04	$4.48^{+0.06}_{-0.05}$
NGC2107	60	10.05 ± 0.13	9.43 ± 0.08	9.20 ± 0.11	$4.01^{+0.04}_{-0.05}$	
NGC2134	60	9.94 ± 0.03	9.50 ± 0.02	9.43 ± 0.02	$3.98^{+0.03}_{-0.04}$	
NGC2156	72	10.81 ± 0.17	10.43 ± 0.22	10.43 ± 0.26	$3.59^{+0.04}_{-0.05}$	3.65 ± 0.08
SMC						
NGC265	62	10.90 ± 0.13	9.88 ± 0.09	9.76 ± 0.12	$3.41^{+0.18}_{-0.30}$	

Notes to Table B10: Column (1) is the cluster identification. Column (2) gives the diameter of the used aperture (to match the optical photometry). J, H and K_S integrated magnitudes with corresponding errors are listed in columns (3) through (5). Column (6) presents an estimate of the stellar mass which contributes to the measured integrated colours. These are typically lower than the total cluster mass. The mass estimates are based on the cluster age, metallicity, observed J band magnitude, and the model predictions of Maraston (2005). Column (7) lists the total mass estimates of the objects in common between present study and McLaughlin & van der Marel (2005).
* No integrated-light optical photometry was recovered from the literature for SL663. NIR measurements are presented for aperture diameter of 60″.

method, Mackey & Gilmore derived metallicities that are consistent with earlier measurements. Grocholski et al. also published [Fe/H]=-1.57 ± 0.03 for Reticulum, which is in very good agreement with [Fe/H]=-1.66 ± 0.12 given by Mackey & Gilmore. The relative ages of the three clusters with respect to MW clusters with a similar metallicity were derived using the techniques of Vandenberg et al. (1990).

B2 Cluster in the 2 Gyr $\leqslant$ Age $<$ 10 Gyr interval

A survey of the literature revealed 15 SMC/LMC clusters in this age range. Their ages and metallicities alongside with the corresponding references are listed in Table B9. Most of the LMC cluster metallicity estimates comes from Grocholski et al. (2006). Their results are based on CaT spectroscopy of multiple stars in each cluster and generally are in a good agreement with earlier studies (e.g. Olszewski et al. 1991). Cluster metallicities based on spectroscopic measurements also agree with the CMD-based metallicity estimates of Kerber et al. (2007). The latter work is the source of the

age and extinction estimates for the majority of the LMC objects.

All six of the SMC clusters included in the $2-10$ Gyr bin fall within the age range between $5-8$ Gyr; no LMC clusters with these ages are known. Most of the information about these SMC clusters was retrieved from the papers of Mighell et al. (1998a,b), based on deep *HST* WFPC2 observations. Metallicities and reddening for the objects were derived applying the S94 method. The age estimates listed in Table B9 are assuming an age of 9.0 Gyr for Lindsay1. Independent estimates of Alcaino et al. (2003) confirm this value. Spectroscopic metallicities for three SMC clusters were recovered from Da Costa & Hatzidimitriou (1998).

Integrated-light NIR photometry and mass estimates for the (2 Gyr $\leqslant$ Age $<$ 10 Gyr) sub-sample are presented in Table B10. We should note that the masses of the LMC objects are in the order of $10^4 \mathcal{M}_\odot$, therefore a relatively large spread relative to the model predictions is not unexpected. Only NGC416 has an estimated mass $> 10^5 \mathcal{M}_\odot$.
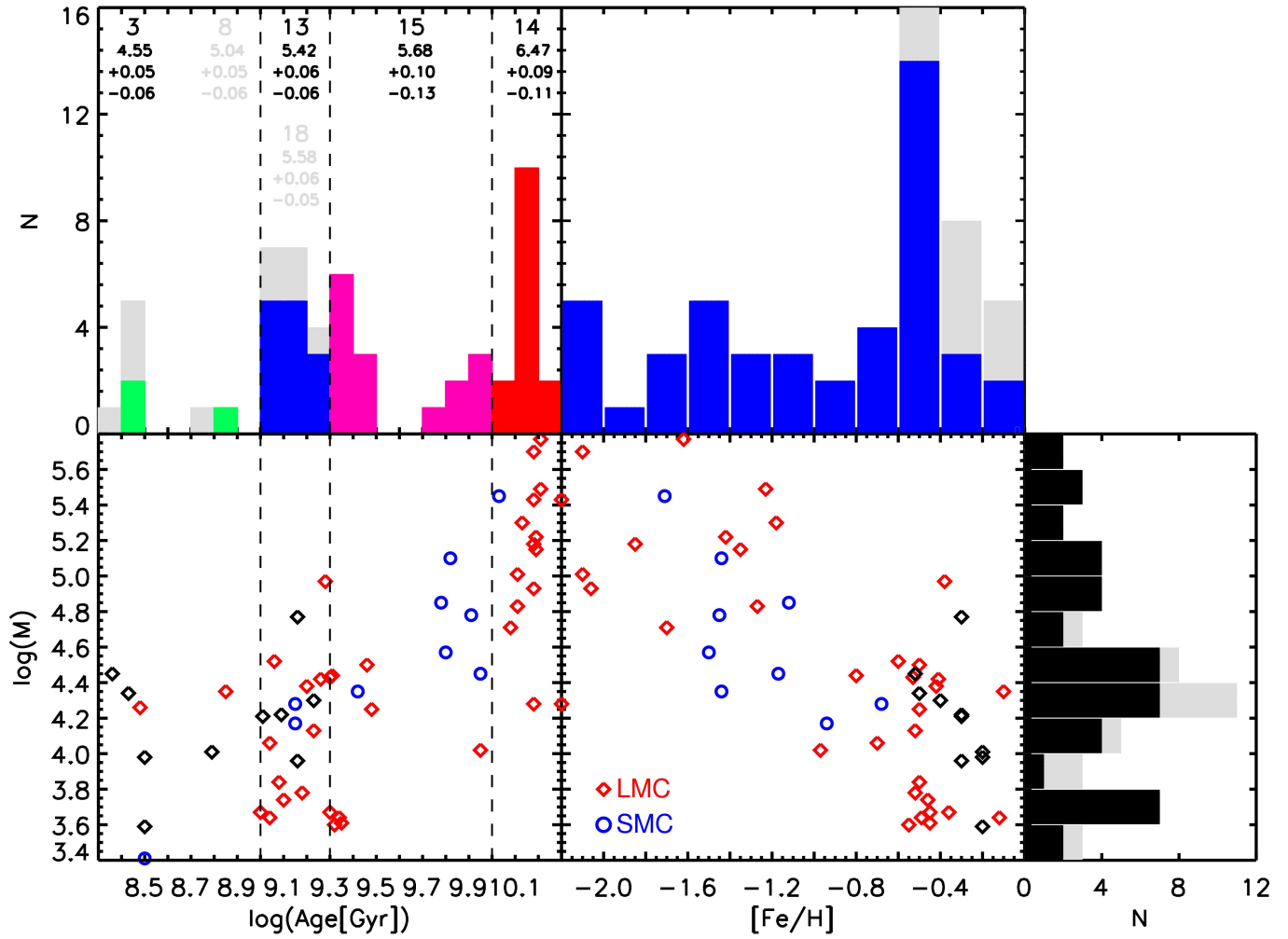
Figure B18. Global properties of our test sample. The cumulative mass and number of objects in each age bin is shown on the age histogram. The objects from the S parameter extension are presented in black and their contribution to the histograms is shown in gray. Also in gray are given the number of objects and total mass for the age bins when the extended sample is taken into account.

B3   Clusters in the 1 Gyr ⩽ Age < 2 Gyr interval

As in the previous section, the bulk of the LMC cluster properties in this age range come from Grocholski et al. (2006) and Kerber et al. (2007). The adopted values are presented in Table B9. Occasionally we supplement age information from Geisler et al. (1997) and metallicity information from Olszewski et al. (1991). The clusters in this age range have sampled stellar masses around $10^4 \mathcal{M}_\odot$, and again some spread is expected in the individual data points. Only NGC 1978 is close to $10^5 \mathcal{M}_\odot$.

Some details on individual clusters in this age interval are provided below. Ferraro et al. (2006) showed that despite its large observed ellipticity and suspected metallicity spread (Alcaíno et al. 1999; Hill et al. 2000), NGC 1978 is not the product of merged clusters. They derived metallicities for 11 gaint stars cluster in NGC 1978 from high-resolution UVES/FLAMES VLT spectroscopy. No significant variations in the giant's metal abundance were found (resulting mean [Fe/H] is listed in Table B9). We conclude that NGC 1978 can be used as a test particle in our analysis. The age of this object was derived by Mucciarelli et al. (2007) applying fit of theoretical isochrones to *HST* ACS

data. Information for the two SMC objects is retrieved from the works of Alves & Sarajedini (1999) and Crowl et al. (2001). Five additional objects were added using the calibration presented in Appendix A.

B4   Clusters in the 200 Myr ⩽ Age < 1 Gyr interval

Based a search of the literature, we only identified three clusters in the 200 Myr−1 Gyr age range, with age estimates based on deep CMDs. In order to expand our test sample, we use the S-parameter recalibration from Appendix A. information. Based on equation A2, five more clusters were added to this age bin. The properties of the sample are also summarized in Table B9.

There are age and metallicity estimates for some of the objects from this sub-sample available in the literature. Dirsch et al. (2000) presented data for six LMC clusters based on CCD Strömgren photometry. We adopt their metallicity estimate for NGC2031.

Information for several more clusters in the 200 Myr - 1 Gyr age interval is available in the recent study of Wolf et
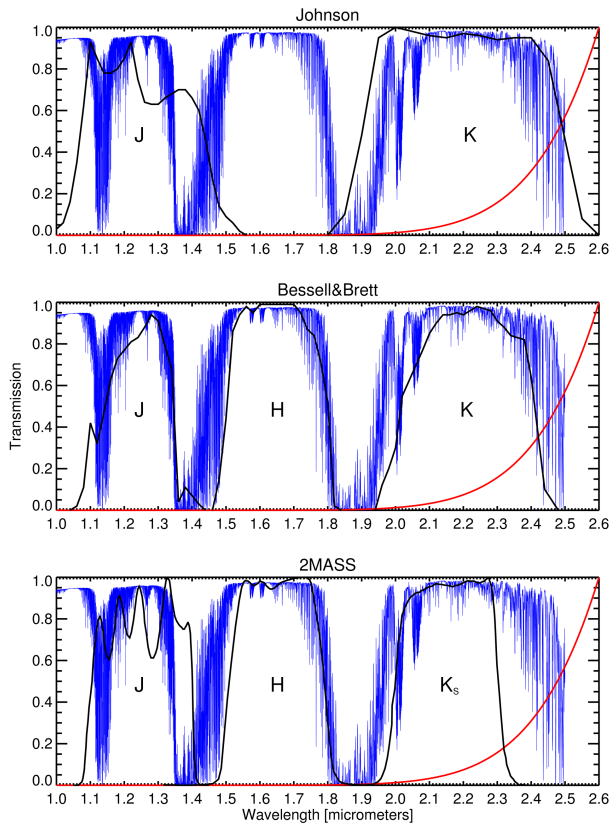
Figure C19. Filter transmission curves of the Johnson (1965), Bessell & Brett (1988) and 2MASS photometric systems. The atmospheric transmission for the south 2MASS facility (CTIO), is plotted in blue. Red represents the thermal emission of the atmosphere at $20°$C (scaled to reach unity at 2.6μm for illustrational purposes). It is obvious that the "K-short" (K_S) filter significantly reduces the influence of the thermal background compared to the Johnson and Bessel & Brett systems. The 2MASS J is broader than the atmospheric window, and the transmission variability was accounted for during the extensive calibration observations. The H filter was introduced to the Johnson 1965 system somewhat later (Johnson 1968) and the transmission curve was never published. The NIR colours for the majority of the SSP models use the filter transmissions of Bessell & Brett (1988).

al. (2007) The authors use Bruzual-Charlot high-resolution stellar population synthesis models to fit the SEDs and simultaneously estimate ages and metallicities of globular clusters in the Magellanic Clouds and M31. Their age results are in a good agreement with our S parameter ages.

APPENDIX C: TRANSFORMATION OF MODEL COLOURS TO THE 2MASS SYSTEM

Today's SSP model predictions for NIR colours are provided in various photometric systems. In order to avoid systematic offsets, observations and model predictions should be compared in the same photometric system.

Johnson (1965) defined a photometric system, in both the optical and NIR, which is currently perhaps the most widely used. Unfortunately however, the NIR passbands of Johnson are broader than the atmospheric transmission win-
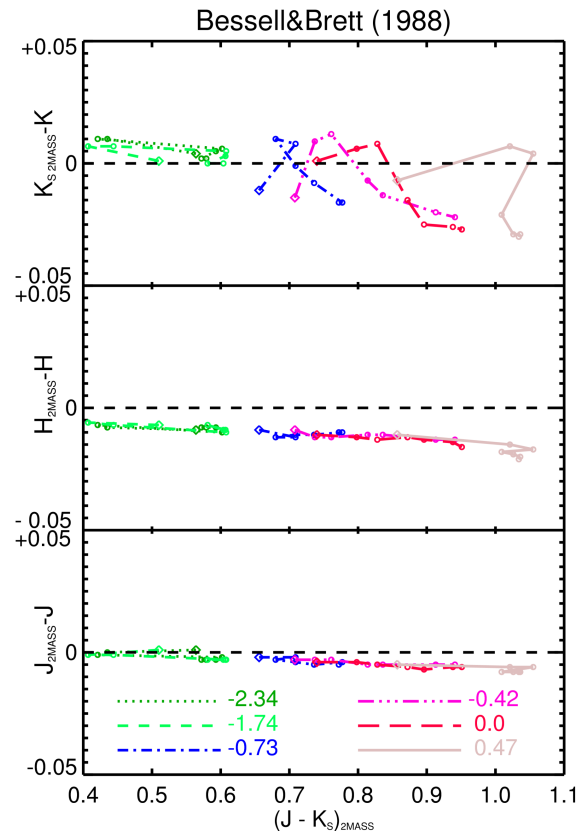

Figure C20. The differences between 2MASS and Bessell & Brett (1988) NIR magnitudes as a function of $(J - K_s)_{2\text{MASS}}$. The dependence of the age and metallicity is also shown (diamonds represent age of 0.2 Gyr for each metallicity (colour coded) and the following circles on the line correspond to 0.5, 1, 2, 5, 10, 15 Gyr respectively). Note the scatter for $K_{s2\text{MASS}} - K$, illustrating the need of independent fits for the different stellar populations.

dows. This can lead to substantial variations in sky background levels (which can also vary on short timescales). Hence there can be significant differences between observations conducted in the original Johnson (1965) filter set and more recent NIR systems, which have been developed to fit within the atmospheric windows and to decrease the thermal background at longer wavelengths (K band).

Bessell & Brett (1988) examined the relations between the NIR photometric systems of several different observatories and introduced a homogenized NIR system based on the works of Glass (1985) and Johnson (1966). The filter transmission curves of the Johnson (1965) and the Bessell & Brett (1988) systems are shown in the top and middle panel of Figure C19. In the bottom panel we plot the 2MASS filter system (Skrutskie et al. 2006). The estimated mean atmospheric transmission for CTIO taken from the online 2MASS All-sky Release Explanatory Supplement[7] and the thermal emission of Earth's atmosphere (blackbody with a temperature of $20°$C) are overplotted in blue and red. Differences between the systems are clearly visible. The 2MASS photometric system by Skrutskie et al. appears to be least affected

---

[7] http : //www.ipac.caltech.edu/2mass/releases/allsky/doc/ sec3_1b1.tbl16.html

Table C5. Transformation coefficients between 2MASS and Bessell & Brett systems for Equations (1), (2), and (3).

[Fe/H]	a_J	b_J	a_H	b_H	a_{K_S}	b_{K_S}
-2.34	-0.011	0.005	-0.008	-0.004	-0.037	0.026
-1.74	-0.014	0.006	-0.015	0.000	-0.023	0.016
-0.73	-0.023	0.012	-0.003	-0.009	-0.100	0.067
-0.42	-0.011	0.005	-0.014	-0.001	-0.098	0.072
0.0	-0.014	0.007	-0.022	0.006	-0.198	0.158
0.47	-0.008	0.001	-0.033	0.017	0.015	-0.029

by the Earth's atmosphere and by the thermal background. It is also clear that observations in these different systems will result in different NIR colours.

The 2MASS system seems to be a natural choice, given the extensive sky coverage and the precise internal photometric calibration. Among the SSP models being considered here, only Bruzual & Charlot (2003) provide 2MASS NIR colours. The other models use NIR passbands on the Bessell & Brett photometric system, although they are sometimes referred to as Johnson JHK passbands. However it is clear that the system of Bessell & Brett (1988) has different filter throughputs from Johnson (as illustrated in Figure C19). Given the advantages of the 2MASS photometric system, we encourage the SSP model builders to provide output in the 2MASS system. For the purposes of the present work we transform the NIR colours predicted by the models to the 2MASS system. To do so, we convolved spectral energy distributions (SEDs) provided by Bruzual & Charlot (2003) with the filter transition curves from Bessell & Brett (1988) and (Skrutskie et al. 2006) using the IRAF/STSDAS SYNPHOT package. Synthetic NIR colours and magnitude differences were derived for a wide age/metallicity parameter space. The differences between the synthetic 2MASS and Bessell & Brett magnitudes as a function of $(J - K_S)_{2MASS}$ colour is presented in Figure C20. It is obvious that different transformation equations should be applied for the different populations as a function of metallicity, especially for K and K_s. We derived a set of transformation equations adequate for our purposes:

$$J_{2MASS} = J_{BB88} + (a_J(J - K)_{BB88} + b_J) \qquad (C1)$$

$$H_{2MASS} = H_{BB88} + (a_H(J - K)_{BB88} + b_H) \qquad (C2)$$

$$K_{S2MASS} = K_{BB88} + (a_{K_S}(J - K)_{BB88} + b_{K_S}) \qquad (C3)$$

The transformation coefficients as function of metallicity are listed in Table C5. These transformations were used to recompute the model colours. As an example the differences between the original and the transformed model grids are shown in $(V - J)$ vs. $(J - K)$ colour-colour space in Figure C21. The grids for the Bessell & Brett (1988) JHK system used by the Maraston (2005), Anders & Fritze-v. Alvensleben (2003), and Vazdekis (1999) models are shown in cyan and the corresponding grids using the 2MASS system are shown in black. We use the 2MASS system for the subsequent analysis.

This paper has been typeset from a TEX/ LATEX file prepared by the author.
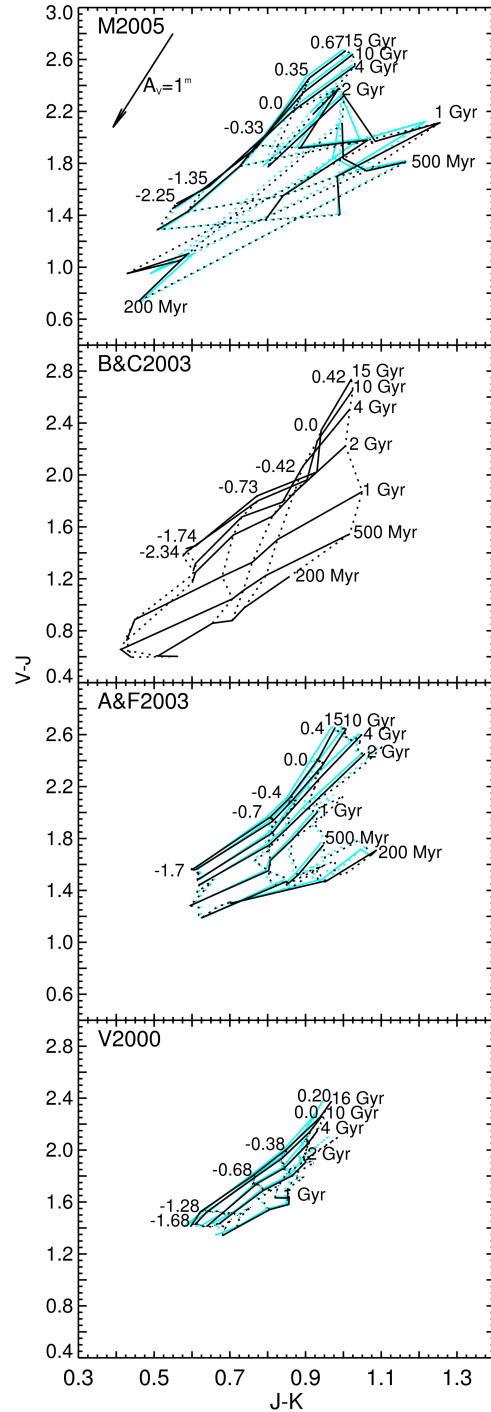

Figure C21. Illustration of the variance of model grids computed in the photometric systems of Bessel & Brett (1988; in cyan) and 2MASS (in black). $(V - J)$ vs. $(J - K)$ (resp. $(J - K_S)$ for 2MASS) for the models of Maraston (M2005), Anders & Fritze (A&F2003) and Vazdekis (V2000) are presented. The models of Bruzual & Charlot (B&C2003) were originally computed in the 2MASS photometric system. The ages are given on the right of the isochrones and the metallicities are labeled along the oldest isochrone for each model. A reddening vector corresponding to one magnitude of visual extinction is shown in the top panel.